

# Exploring Hybrid Star Models with Quark and Hadronic Matter in $f(Q)$ Gravity

M. Sharif<sup>1,2\*</sup> and Madiha Ajmal<sup>1†</sup>

<sup>1</sup> Department of Mathematics and Statistics, The University of Lahore,  
1-KM Defence Road Lahore-54000, Pakistan.

<sup>2</sup> Research Center of Astrophysics and Cosmology, Khazar University,  
Baku, AZ1096, 41 Mehseti Street, Azerbaijan.

## Abstract

In this paper, we develop a model for a static anisotropic hybrid star that includes strange quark matter and hadronic matter. We solve the field equations in the  $f(Q)$  gravity framework (where  $Q$  is the non-metricity) using the Finch-Skea metric. The relationship between density and pressure for strange quark matter is described using the MIT bag model equation, while for hadronic matter, the radial pressure and density are related by a linear equation of state. We select the compact star EXO 1785-248 and analyze five different values of the coupling constant. To evaluate the physical feasibility of the model, we perform a graphical analysis of key properties, including the metric components, energy density, radial and tangential pressures, anisotropy, gradients, quark matter density and pressure, the equation of state parameter, energy conditions and the mass function. We further examine the stability and equilibrium of the star through parameters such as compactness, redshift, causality conditions, Herrera cracking, the adiabatic index and the Tolman-Oppenheimer-Volkoff equation. We observe that  $f(Q)$  gravity effectively describes the macroscopic properties of hybrid stars.

---

\*msharif.math@pu.edu.pk (Corresponding author)

†madihaajmal222@gmail.com

**Keywords:** Hybrid star;  $f(Q)$  gravity; Stellar configurations.

**PACS:** 97.60.Jd; 04.50.kd; 97.10.-q.

## 1 Introduction

General Relativity (GR) has been a powerful and reliable framework for understanding gravity. However, observations of the rapid expansion of the universe have revealed certain limitations of GR. In addition to the universe's accelerated expansion, several other observational and theoretical issues also highlight the limitations of GR. For example, the rotation curves of galaxies cannot be explained by GR without assuming the existence of dark matter. Similarly, anomalies in gravitational lensing, cosmic microwave background data and large scale structure formation challenge the completeness of GR. Moreover, GR breaks down near singularities such as in black holes and is not renormalizable in quantum field theory. These issues collectively motivate the exploration of modified gravity theories (MGTs) as potential extensions or alternatives to GR [1]. The accelerated expansion is a pivotal aspect of the history of the universe, prompting questions about the mysterious force responsible for it. Since GR alone does not fully explain this phenomenon, scientists are exploring new theories to solve this mystery [2].

There are two main approaches to explain the universe accelerated expansion. The first approach suggests modifying the universe composition by introducing new elements, like dark energy (DE). Dark energy is characterized by high negative pressure and remains undetected in direct observations. Einstein introduced the cosmological constant ( $\Lambda$ ) in his equations as a leading candidate for DE. It aligns well with current observations, though it also presents some theoretical challenges. The second approach is to modify GR itself through MGTs. Recent experiments and observations indicate that some MGTs effectively describe both the early universe inflation and later-period acceleration. With these two approaches, scientists aim to understand the accelerated expansion and possibly unveil hidden aspects of the universe.

In GR, gravity is explained through the Ricci scalar ( $R$ ), which arises from Riemannian geometry based on the curvature of spacetime. An extension of GR, known as  $f(R)$  gravity, generalizes the theory by replacing  $R$  with an arbitrary function of  $R$ . The GR traditionally relies on the curvature of the Levi-Civita connection [3], which is free from torsion. Other gravitational theories, such as the teleparallel equivalent of GR (TEGR) [4],

replaces curvature with torsion  $\mathcal{T}$ , leading to a modified version known as  $f(\mathcal{T})$  gravity. Yet another approach is symmetric teleparallel gravity (STG) [5], which describes gravity via the non-metricity, eliminating both curvature and torsion. Extending this framework,  $f(Q)$  gravity [6] replaces  $Q$  with a general function of  $Q$ , opening new possibilities for understanding gravitational phenomena, especially in cosmology and astrophysics. This theory has attracted attention to explain cosmic acceleration and other large-scale cosmic dynamics [7].

From an astrophysical and cosmological point of view,  $f(Q)$  gravity offers several distinct advantages over more commonly studied MGTs such as  $f(R)$  and  $f(\mathcal{T})$  gravity theories. These theories offer innovative frameworks for understanding the complex structures of hybrid stars, which consist of a mixture of strange quark matter and hadronic matter. While  $f(R)$  and  $f(\mathcal{T})$  gravity theories have been extensively explored to address various cosmic phenomena,  $f(Q)$  gravity introduces key advantages, particularly in modeling extreme stellar environments and handling anisotropic pressures. The  $f(R)$  theory has been successful in addressing large-scale cosmic issues such as DE and the expansion of the universe [8], it faces challenges when it comes to modeling singularities and exotic matter states, particularly in the context of stellar interiors [9]. Similarly,  $f(\mathcal{T})$  gravity [10], which is based on torsion instead of curvature, offers a distinct perspective on gravitational dynamics [11] but struggles to handle the complexity of hybrid star interiors in the same way  $f(Q)$  does.

One widely studied theory is  $f(Q)$  gravity, which has shown broad potential in making predictions about both astrophysical and cosmological phenomena. Anagnostopoulos et al. [12] introduced a new  $f(Q)$  model that, while similar to  $\Lambda$ CDM in parameters, offers unique cosmological behavior. Frusciante [13] examined a model within this theory that resembles the large-scale behavior of the  $\Lambda$ CDM model but shows unique characteristics at the level of linear perturbations. Mandal et al. [14] studied how bulk viscosity impacts cosmological models. Wang et al. [15] studied spherically symmetric fluid spheres in this theory, finding that a Schwarzschild anti-de Sitter solution exists but an exact Schwarzschild solution is not possible for nontrivial  $f(Q)$  functions. D'Ambrosio et al. [16] developed perturbative corrections for Schwarzschild solutions in this gravity, incorporating extra characteristics arising from the dynamic affine connection. Gadbail et al. [17] proposed various  $f(Q)$  gravity models, demonstrating that  $Q$  can replicate the observed accelerated cosmic expansion similar to  $\Lambda$ CDM. Recent papers [18]

have extensively examined  $f(Q)$  gravity, investigating various geometrical and physical aspects of this theory.

A hybrid star is a unique astrophysical object that combines the properties of neutron stars and quark stars, representing a transitional phase between the two. These stars emerge when a massive star undergoes gravitational collapse after exhausting its nuclear fuel, leading to the formation of a dense neutron rich core. In the core of a hybrid star, the density becomes so extreme that neutrons are decomposed into their constituent quarks, resulting in a state known as deconfined quark matter. This quark matter often includes strange quarks, further emphasizing the hybrid nature of the star. The outer layers of a hybrid star remain similar to those of a traditional neutron star, composed primarily of nuclear matter such as neutrons and protons bound by strong nuclear forces. This unique composition makes hybrid stars essential for studying matter under extreme conditions, compact objects and high energy astrophysical phenomena. Among the models, the conventional hybrid star featuring quark matter at the core and neutron matter in the crust is preferred due to its alignment with observational data, including GW170817 tidal deformability constraints, NICER radius measurements and massive pulsar masses. In contrast, the inverted hybrid model [19], with hadronic matter at the core and quark matter in the crust, relies on speculative assumptions such as quark matter stability at low pressures, which lacks observational confirmation. Thus, the conventional model stands out for its reliability, extensive study and compatibility with astrophysical constraints.

Mishra et al. [20] analyzed neutron-quark phase transitions in hybrid quark stars, finding stable, predominantly quark matter stars with a neutron crust by solving Tolman-Oppenheimer-Volkoff equations. Khadkikar et al. [21] studied neutron-to-quark matter phase transitions in hybrid stars using a relativistic confinement model, achieving stable solutions. Maheswari et al. [22] proposed an equation of state (EoS) incorporating spin-isospin forces, aligning well with unpolarized nuclear matter. This EoS predicts a ferromagnetic transition in neutron matter at high densities and effectively models the mass, size and magnetic fields of hybrid stars. Schertler et al. [23] examined medium effects in quark matter, finding that they reduced the pure quark matter core in hybrid stars, favoring a mixed quark-hadronic phase across various strong coupling constants. Blackman et al. [24] explored the effect of star-disk magnetohydrodynamic winds on planetary nebulae, proposing that disk-dominated winds and magnetic shaping explain multi-polar structures. Gupta et al. [25] studied the impact of the quark-nuclear matter mixed

phase on radial oscillation modes in hybrid stars using relativistic mean-field theory and realistic nucleon interactions. Grigorian et al. [26] derived EoS for quark matter using a nonlocal chiral quark model, emphasizing diquark condensation's impact on color superconductivity and hybrid star stability.

Alford et al. [27] explored how hybrid stars resemble the mass-radius relationship of purely nucleonic stars using realistic EoS. Nicotra et al. [28] investigated the hadron-quark phase transition in protoneutron stars, finding maximum masses under 1.6 solar masses. Hussain et al. [29] synthesized hybrid fluorinated star polymers, resulting in enhanced thermal stability, spherical particle formation and improved surface properties. Dexheimer et al. [30] demonstrated that high magnetic fields alter the particle composition, structure and anisotropy of hybrid stars. Alford et al. [31] studied hybrid star mass-radius curves, finding conditions where hybrid stars exceed 2 solar masses. Bhar [32] proposed a new hybrid star model that matches observational mass data and requires negative surface pressure for stability. Burgio and Zappala [33] analyzed the color-flavor locking phase in hybrid star quark cores, noting its phase transition features and the influence of hyperons on mass-radius relations. Kaltenborn et al. [34] proposed a hybrid EoS with excluded volume effects, predicting third-family compact stars meeting the  $2M_\odot$  constraint. Nandi and Char [35] found that the GW170817 tidal deformability constraint limits MIT bag model parameters and sets upper radius limits for 1.4 and  $1.6 M_\odot$  hybrid stars. Khanmohamadi et al. [36] found that hybrid star models with hadron-quark phase transitions satisfy GW170817 constraints on radii and tidal deformability, achieving stable high-mass configurations. Recent studies have made significant advancements in understanding hybrid stars [37].

The study of hybrid stars in MGT is crucial due to their unique environments, which provide insights into extreme astrophysical phenomena. These stars, composed of quark and hadronic matter, exist at densities exceeding nuclear levels, offering a natural laboratory to explore high-density matter and the hadronic-to-quark phase transition. MGTs, which extend GR to address challenges like DE and the universe's accelerated expansion, enable researchers to investigate gravity in strong-field regimes. In this context, MGT predicts solutions that avoid singularities, proposing smooth core structures for hybrid stars, which differ from the predictions of GR. Observational data on hybrid star's masses, radii and structures further refine our understanding of gravity in extreme conditions, bridging weak and strong gravitational fields. Abbas and Nazar [8] studied stable, singularity-free anisotropic com-

pact stars with quark and hadronic matter under  $f(R)$  gravity, using the bag model EoS. Bhar et al. [38] investigated quark deconfinement in hybrid star cores, modeling phase transitions and analyzing the impact of bag pressure on star structure, with findings compared to observational data. Rej [39] examined a hybrid stellar model of quark and hadronic matter in modified  $f(G)$  gravity ( $G$  denotes the Gauss-Bonnet invariant term) and evaluated its physical validity for the compact star 4U 1538-52.

The Finch-Skea metric has an important role for modeling compact stars in four or higher dimensional spacetime. Its non-singular and practical properties make it widely adopted in compact star modeling, leading to its frequent applications in compact stellar objects with various forms of matter. This metric has been extensively used to examine gravastars, wormholes, neutron stars, hybrid stars and strange stars in both GR and alternative gravity theories. Finch and Skea [40] developed a new mathematical model (metric) for describing spherical, symmetric, compact stars. Later, this Finch-Skea metric was adapted to four dimensions to create models of stars with uneven (anisotropic) pressures [41]. Sharma and Ratanpal [42] used the Finch-Skea metric to propose a model for relativistic stars. Sharma and Das [43] explored Bessel function-based solutions for anisotropic systems within the Finch-Skea spacetime. Pandya et al. [44] expanded the Finch-Skea framework to propose new solutions for spherically symmetric anisotropic matter, showing compatibility with various compact stars. Molina et al. [45] demonstrated that static fluid solutions in pure Lovelock gravity exhibit universal behavior across dimensions, unifying stellar interior models from the compact Schwarzschild to Finch-Skea states. Banerjee et al. [46] examined how DE affects compact astrophysical objects using the Finch and Skea ansatz to solve Einstein equations.

Dayanandan et al. [47] explored a modified Finch-Skea anisotropic configuration within Class I spacetime by employing gravitational decoupling to construct viable models of compact stars. Gul et al. [48] assessed the physical acceptability and stability of anisotropic stellar models in  $f(Q)$  gravity using Finch-Skea geometry, validating the models through several stability checks. Mustafa et al. [49] analyzed the behavior of a static, spherically symmetric anisotropic star under the framework of  $f(Q)$  theory by incorporating the Karmarkar condition along with the Finch-Skea structure. Rej et al. [50] employed the complexity factor approach with a Finch-Skea background to develop a relativistic model of an anisotropic DE star. Shahzad et al. [51] proposed a new solution in Rastall gravity coupled with a quintessence field,

applying the Finch-Skea framework to study isotropic compact stars. Das et al. [52] examined anisotropic relativistic configurations with the Finch-Skea metric, particularly focusing on applications to the pulsar PSR J0348+0432.

In this study, we focus on developing a hybrid star model within the framework of  $f(Q)$  gravity to incorporate recent observations of compact stars. The paper is organized as follows. Section 2 provides an overview of  $f(Q)$  gravity and also discusses the internal spacetime. Section 3 solves the field equations using the Finch and Skea ansatz metric. Section 4 explains the connection between the inner spacetime and the outer Schwarzschild vacuum solution at the boundary  $r = \mathcal{R}$  and expresses the metric constants in terms of the star's mass and radius. In sections 5 and 6, we discuss some physical properties and stability of the model, respectively. Section 7 presents the summary of the results obtained.

## 2 Formulation of $f(Q)$ Gravity

The affine connection  $\hat{\Gamma}_{\nu\varsigma}^\mu$  in the framework of  $f(Q)$  gravity can be expressed as a combination of three independent components [53]

$$\hat{\Gamma}_{\nu\varsigma}^\mu = \Gamma_{\nu\varsigma}^\mu + K_{\nu\varsigma}^\mu + \mathbb{L}_{\nu\varsigma}^\mu. \quad (1)$$

where  $\Gamma_{\nu\varsigma}^\mu$  is the Levi-Civita connection,  $K_{\nu\varsigma}^\mu$  is the contortion tensor and  $\mathbb{L}_{\nu\varsigma}^\mu$  is the disformation tensor. The contortion tensor is defined as

$$K_{\nu\varsigma}^\mu = \hat{\Gamma}_{[\nu\varsigma]}^\mu + g^{\mu\sigma} g_{\nu\kappa} \hat{\Gamma}_{[\varsigma\sigma]}^\kappa + g^{\mu\sigma} g_{\varsigma\kappa} \hat{\Gamma}_{[\nu\sigma]}^\kappa, \quad (2)$$

while the disformation tensor is given by

$$\mathbb{L}_{\nu\varsigma}^\mu = \frac{1}{2} g^{\mu\sigma} (Q_{\varsigma\nu\sigma} + Q_{\nu\varsigma\sigma} - Q_{\mu\nu\varsigma}), \quad (3)$$

with the non-metricity tensor defined as  $Q_{\varsigma\nu\sigma} = \nabla_\sigma g_{\nu\varsigma}$ . The Levi-Civita connection can be written as

$$\Gamma_{\nu\varsigma}^\mu = \frac{1}{2} g^{\mu\sigma} (g_{\sigma\varsigma,\nu} + g_{\sigma\nu,\varsigma} - g_{\nu\varsigma,\sigma}), \quad (4)$$

and in the context of STG, it is related to the disformation tensor by

$$\Gamma_{\nu\varsigma}^\mu = -\mathbb{L}_{\nu\varsigma}^\mu. \quad (5)$$

The gravitational action in non-covariant form is expressed as

$$S = \frac{1}{2\kappa} \int g^{\nu\varsigma} (\Gamma_{\sigma\nu}^{\iota} \Gamma_{\varsigma\iota}^{\sigma} - \Gamma_{\sigma\iota}^{\iota} \Gamma_{\nu\varsigma}^{\sigma}) \sqrt{-g} d^4x, \quad (6)$$

where  $\kappa$  is the gravitational coupling constant, defined as  $\kappa = 8\pi G$ , with  $G$  being the gravitational constant. Using Eq.(5), the action becomes

$$S = -\frac{1}{2\kappa} \int g^{\nu\varsigma} (\mathbb{L}_{\sigma\nu}^{\iota} \mathbb{L}_{\varsigma\iota}^{\sigma} - \mathbb{L}_{\sigma\iota}^{\iota} \mathbb{L}_{\nu\varsigma}^{\sigma}) \sqrt{-g} d^4x. \quad (7)$$

which corresponds to the action of STG. In this study, we adopt the coincident gauge, in which the affine connection  $\hat{\Gamma}_{\nu\varsigma}^{\mu}$  vanishes identically. This gauge choice is standard in STG and simplifies the formulation by rendering the connection's equations of motion trivial. As a result, only the metric degrees of freedom contribute dynamically, while the connection does not introduce additional dynamics. This simplification is justified for the current static, spherically symmetric stellar model, and we clearly state that the effects of connection dynamics are not considered in this work. The action for  $f(Q)$  gravity can be expressed as [6]

$$S = \int \left( \frac{1}{2\kappa} f(Q) + \mathcal{L}_m \right) \sqrt{-g} d^4x, \quad (8)$$

where  $g$  denotes the determinant of the metric tensor,  $\mathcal{L}_m$  is the Lagrangian density for matter. The field equations for  $f(Q)$  gravity are then given by

$$\frac{-2}{\sqrt{-g}} \nabla_{\mu} (f_Q \sqrt{-g} P_{\gamma\psi}^{\mu}) - \frac{1}{2} f g_{\gamma\psi} - f_Q (P_{\gamma\mu\nu} Q_{\psi}^{\mu\nu} - 2 Q^{\mu\nu} \gamma P_{\mu\nu\psi}) = \kappa T_{\gamma\psi}, \quad (9)$$

where all relevant terms are detailed in Appendix A and  $f_Q = \frac{\partial f(Q)}{\partial Q}$ .

We model the star interior spacetime using a static, self-gravitating sphere defined by

$$ds_-^2 = e^{\alpha(r)} dt^2 - e^{\beta(r)} dr^2 - r^2 (d\theta^2 - \sin^2 \theta d\phi^2), \quad (10)$$

where minus sign denotes the interior spacetime. This setup allows us to describe the inner structure of a self-gravitating object in a co-moving frame, where the fluid inside the star behaves as an anisotropic relativistic fluid. The study considers a hybrid star that contains two types of matter: hadronic matter and strange quark matter. This model is based on the idea that

under certain conditions within a star, a phase transition might occur, where normal nuclear matter changes into strange quark matter [54]. The energy-momentum tensor (EMT) associated with the two-fluid model is given by the following notation

$$T_0^0 = \rho + \rho_q, \quad T_1^1 = -(p_r + p_q), \quad T_2^2 = T_3^3 = -(p_t + p_q), \quad (11)$$

where,  $\rho$ ,  $p_r$  and  $p_t$  represent the density, radial pressure and tangential pressure, respectively, while  $\rho_q$  and  $p_q$  denote the density and pressure associated with quark matter. The field equations for a hybrid star in  $f(Q)$  gravity can be expressed as

$$\begin{aligned} \kappa(\rho + \rho_q) &= \frac{e^{-\beta}}{2r^2} \left[ f_Q \left( (e^\beta - 1)(2 + r\alpha') + (1 + e^\beta)r\beta' \right) + fr^2 e^\beta \right. \\ &\quad \left. + 2rf_{QQ}Q'(e^\beta - 1) \right], \end{aligned} \quad (12)$$

$$\begin{aligned} \kappa(p_r + p_q) &= -\frac{e^{-\beta}}{2r^2} \left[ f_Q \left( (e^\beta - 1)(2 + r\beta' + r\alpha') - 2r\alpha' \right) + fr^2 e^\beta \right. \\ &\quad \left. + 2rf_{QQ}Q'(e^\beta - 1) \right], \end{aligned} \quad (13)$$

$$\begin{aligned} \kappa(p_t + p_q) &= \left[ f_q \left( 2\alpha'(e^\beta - 2) - r\alpha'^2 + \beta'(2e^\beta + r\alpha') - 2r\alpha'' \right) + 2fr e^\beta \right. \\ &\quad \left. - 2rf_{QQ}Q'\alpha' \right] \frac{-e^{-\beta}}{4r}, \end{aligned} \quad (14)$$

where prime symbol denotes a derivative with respect to the radial coordinate  $r$ . The scalar  $Q$  becomes

$$Q = \frac{1}{r}(e^{-\beta} - 1)(\alpha' + \beta'), \quad (15)$$

where  $\alpha'$  and  $\beta'$  denote the derivatives of the metric functions  $\alpha(r)$  and  $\beta(r)$ , respectively, with respect to the radial coordinate  $r$ .

The quadratic form of  $f(Q)$  gravity has garnered significant attention due to its potential to describe diverse phenomena in cosmology and astrophysics. Mandal et al. [55] showed that the  $f(Q)$  gravity theory was validated by energy conditions, which constrained  $f(Q)$  models to those consistent with the universe accelerated expansion. Khyllep et al. [56] revealed  $\Lambda$ CDM-like dynamics in  $f(Q) = Q + \alpha Q^n$  gravity, along with deviations in matter growth

and integrability. Lin and Zhai [57] investigated the  $f(Q) = Q + \alpha Q^2$  model, showing its capability to support higher stellar masses with negative modifications while reducing them with positive ones. Zhao [58] explored the conflict between gauge choices and symmetry-based coordinate systems, focusing on the quadratic model within this framework. We adopt a quadratic form of  $f(Q)$  gravity to describe hybrid stars. This is expressed as

$$f(Q) = Q + \zeta Q^2, \quad (16)$$

where  $\zeta$  is a coupling constant that influences the gravity model and its unit is  $L^2$ . We have chosen this form because it is simple and mathematically manageable, effectively describing the properties of compact stars such as hybrid stars. This form combines linear and quadratic terms, providing deeper insight into gravitational effects and the structure of such stars.

### 3 Model of Hybrid Star

We consider the Finch-Skea metric potentials which are given as [40]

$$e^{\alpha(r)} = \left( \xi + \frac{1}{2} r \varphi \sqrt{r^2 \chi} \right)^2, \quad e^{\beta(r)} = r^2 \chi + 1, \quad (17)$$

where  $\xi$ ,  $\varphi$  and  $\chi$  are unspecified, non-zero constants. To complete the system, an additional constraint is required, i.e., a well-founded relationship between  $p_r$  and  $\rho$  of hadronic matter. There are multiple ways to express this relationship. In our model, we adopt a linear EoS defined by

$$p_r = s\rho - h, \quad (18)$$

where  $0 < s < 1$  with  $s \neq 1/3$ , and  $h > 0$ . This EoS has been used by various authors to model compact stars [59], providing a solid basis for our approach. We also assume that the pressure-density relationship for quark matter is described by the MIT bag model EoS [60]

$$p_q = \frac{1}{3}(\rho_q - 4\mathcal{B}_g), \quad (19)$$

where  $\mathcal{B}_g$  represents the bag constant in units of  $MeV/fm^3$  [61]. Witten [62] suggested that strange quark matter could be the true ground state of

strongly interacting matter. Farhi and Jaffe [63] supported this idea, showing that it holds for massless, non-interacting quarks when the bag constant ranges between 57 and 94  $MeV/fm^3$ . The main difference between Eq.(18) and Eq.(19) lies in their physical context. Eq.(18) is a general linear EoS used to model various types of compact stars, with  $s$  and  $h$  providing flexibility to describe different stellar matter. In contrast, Eq.(19) specifically describes quark matter, derived from the MIT bag model, where the bag constant  $\mathcal{B}_g$  has a direct physical meaning related to quantum chromodynamics (QCD) vacuum properties.

The linear EoS and MIT bag model [64] are widely used due to their simplicity and reliability in modeling compact stars, particularly quark-hadron phase transitions and hybrid stars. While advanced models like the polytropic EoS, Nambu-Jona-Lasinio model [65] and perturbative QCD [66] offer detailed microscopic insights and nonlinear behavior, they are often more complex and computationally demanding. Different models influence mass-radius relationships, stability, and thermal evolution but the MIT bag model's adjustable parameters and phenomenological approach make it practical for studying observed phenomena such as tidal deformability from GW170817. This balance between simplicity and accuracy makes it a preferred choice for this study.

With these assumptions understood, we are now ready to solve the field equations and derive expressions for the matter density and pressure associated with regular hadronic matter as well as the density and pressure associated with quark matter. The expressions can be found in Appendix B.

## 4 Boundary Conditions

To ensure that spacetime remains continuous both inside and outside the star model, it is essential for the inner and outer regions to align at the boundary  $r = \mathcal{R}$ . Since we are dealing with a static, non-rotating, spherically symmetric spacetime, the outer region is represented by the de Sitter Schwarzschild vacuum solution, given by the following line element

$$ds_+^2 = \left(1 - \frac{2M}{r} + \frac{\Lambda r^2}{3}\right) dt^2 - \left(1 - \frac{2M}{r} + \frac{\Lambda r^2}{3}\right)^{-1} dr^2 - r^2(d\theta^2 + \sin^2 \theta d\phi^2). \quad (20)$$

Here, plus sign indicates the exterior spacetime and  $M$  is the total mass contained within the boundary of the compact star for the inner region.

Substituting the value from Eq.(17) into (10), we have

$$ds_-^2 = e^{\left(\xi + \frac{1}{2}r\varphi\sqrt{r^2\chi}\right)^2} dt^2 - e^{(r^2\chi+1)} dr^2 - r^2(d\theta^2 + \sin^2\theta d\phi^2). \quad (21)$$

Since the cosmological constant is extremely small ( $\Lambda = 1.105610^{-46} km^{-2}$ ) [67], we can ignore it in our calculations. To connect the star internal spacetime with the external spacetime at the boundary, we must ensure that  $g_{tt}$  and  $g_{rr}$  and  $\frac{\partial}{\partial r}(g_{tt})$  are continuous across the boundary  $r = \mathcal{R}$ . This requirement provides a set of equations as shown below. This approach has been applied in previous studies [68]. We identify these constants specific to the Schwarzschild solution by matching the temporal and radial components of the metric from Eqs.(20) and (21). We can conclude that

$$1 - \frac{2M}{\mathcal{R}} = \left(\xi + \frac{1}{2}\mathcal{R}\varphi\sqrt{\mathcal{R}^2\chi}\right)^2, \quad (22)$$

$$\left(1 - \frac{2M}{\mathcal{R}}\right)^{-1} = \mathcal{R}^2\chi + 1. \quad (23)$$

Differentiating Eq.(22) with respect to  $\mathcal{R}$ , it follows that

$$\frac{2M}{\mathcal{R}^2} = \frac{1}{2}\varphi\left(\mathcal{R}^3\varphi\chi + 2\xi\sqrt{\mathcal{R}^2\chi}\right). \quad (24)$$

We solve these equations together to find expressions for  $\chi$ ,  $\xi$  and  $\varphi$  as follows

$$\chi = \frac{2M}{\mathcal{R}^2(\mathcal{R} - 2M)}, \quad (25)$$

$$\xi = \frac{\sqrt{\frac{M}{\mathcal{R}-2M}}(2\mathcal{R} - 5M)}{2\sqrt{M}\sqrt{\mathcal{R}}}, \quad (26)$$

$$\varphi = \frac{\sqrt{M}}{\sqrt{2}\mathcal{R}^{3/2}}. \quad (27)$$

Following O'Brien and Synge's method [69] for an anisotropic fluid sphere, the radial pressure must be continuous at the boundary of the star, i.e.,  $p_r(\mathcal{R} - 0) = p_r(\mathcal{R} + 0)$ . Since there is no matter outside the stellar surface, the radial pressure just beyond the boundary vanishes, implying  $p_r(\mathcal{R} + 0) = 0$ . Consequently, we set  $p_r(\mathcal{R} - 0)$  at the surface. The full form of the resulting boundary condition, obtained by substituting the expressions for  $B_1$  and  $B_2$

Table 1: Values of  $\chi(km^{-2})$ ,  $\xi(km^{-2})$  and  $\varphi$  for various compact stars.

| Star         | OM $\mathcal{M}_\odot$ | OR km            | EM   | ER  | $\chi$ | $\xi$  | $\varphi$ |
|--------------|------------------------|------------------|------|-----|--------|--------|-----------|
| EXO 1785-248 | $1.3 \pm 0.2$          | $8.85 \pm 0.4$   | 1.2  | 9.2 | 0.0063 | 0.0050 | 0.7790    |
| Vela X-1     | $1.77 \pm 0.08$        | $9.56 \pm 0.08$  | 1.77 | 9.5 | 0.0106 | 0.0112 | 1.9802    |
| SMC X-4      | $1.29 \pm 0.05$        | $8.831 \pm 0.09$ | 1.29 | 8.8 | 0.0082 | 0.0057 | 1.2413    |
| LMC X-4      | $1.04 \pm 0.09$        | $8.301 \pm 0.2$  | 1.04 | 8.3 | 0.0073 | 0.0046 | 0.7625    |
| 4U 1538-52   | $0.87 \pm 0.07$        | $7.866 \pm 0.21$ | 0.87 | 7.8 | 0.0072 | 0.0042 | 0.6129    |

into Eq.(18), is quite lengthy and has therefore been relocated to Appendix C for completeness. This expression governs the behavior of the system under the modified equation of state and plays a fundamental role in the structure equations developed in the subsequent sections.

The constants in the metric coefficients for various compact stars (EXO 1785-248 [70], Vela X-1 [71], SMC X-4 [71], LMC X-4 [71], 4U 1538-52 [71]) are presented in Table 1. In this table, OM denotes the observed mass, OR represents the observed radius, EM indicates the estimated mass and ER corresponds to the estimated radius.

## 5 Physical Analysis

In this section, we investigate the viability of hybrid stars by examining the key physical properties of EXO 1785-248. This star has been chosen because it serves as an excellent example of a hybrid star candidate. Its intense X-ray emissions and unique binary dynamics make it stand out, with a perfect balance of features like matter transfer and gravitational interactions. Additionally, its graphical representation highlights the suitability of the model for studying such systems. These properties include metric components,  $\rho$ ,  $p_r$ ,  $p_t$  and anisotropy, gradients of  $\rho$ ,  $p_r$ ,  $p_t$ , density and pressure of quark matter, EoS parameter, energy conditions, mass-radius function. For all graphical analyses, we use the parameter values  $\zeta = 2, 2.2, 2.4, 2.6, 2.8$ ,  $k = 8\pi$  and  $\mathcal{B}_g = 67 MeV/fm^3$  to illustrate the results.

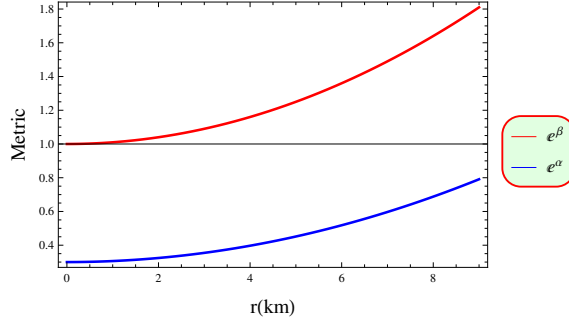


Figure 1: Graph of Metric versus  $r$ .

## 5.1 Metric Components

Metric potentials are key elements in the geometry of spacetime in GR and MTGs. They are essential for modeling dense astrophysical objects. Figure 1 shows that both metric potentials,  $e^\alpha$  and  $e^\beta$ , are plotted against  $r$ . This indicates that both potentials increase steadily with  $r$ .

## 5.2 Behavior of $\rho$ , $p_r$ , $p_t$ and Anisotropy

For our model to be physically plausible, the density  $\rho$ , radial pressure  $p_r$ , and tangential pressure  $p_t$  must remain positive throughout the interior of the fluid sphere. These values should also decrease steadily with increasing radius and be finite at the star's boundary. To verify this, we analyze the graphical behavior of density and pressure in Figure 2. This shows that both density and pressures are positive within the star, with no physical or geometric singularities in the model. Figure 3 illustrates how radial and transverse pressures relate to density. It shows that both pressures increase linearly with density, depending on different values of  $\zeta$ . The pressure anisotropy, defined as  $\Delta = p_t - p_r$ , may be positive (when  $p_t > p_r$ ) or negative (when  $p_t < p_r$ ). Anisotropy is significant in compact star models. Figure 4 reveals that in this model, radial pressure exceeds tangential pressure, resulting in negative anisotropy, which creates an inward-directed attractive force.

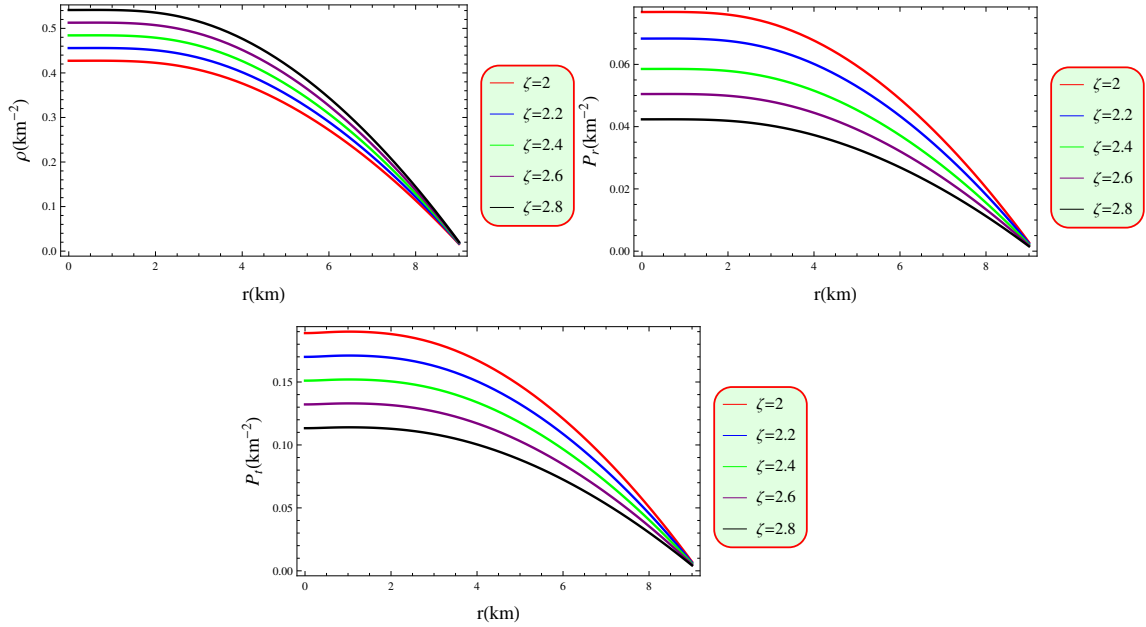


Figure 2: Plots of  $\rho$ ,  $p_r$  and  $p_t$  against  $r$ .

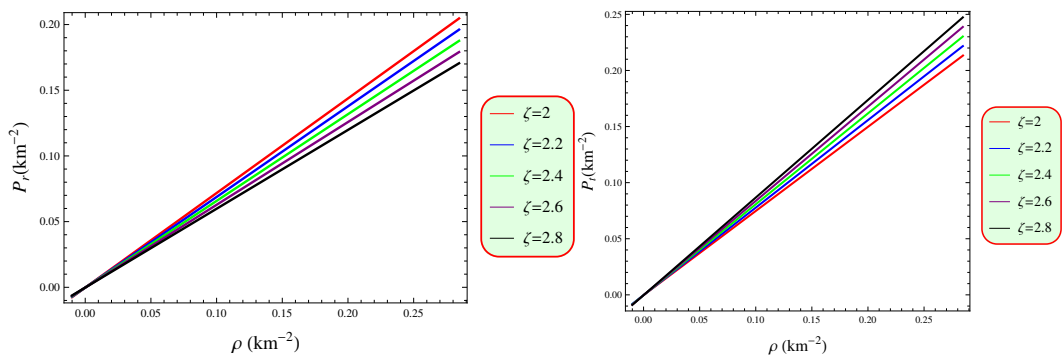


Figure 3: Graphs of relationship between  $p_r$  and  $p_t$  with  $\rho$ .

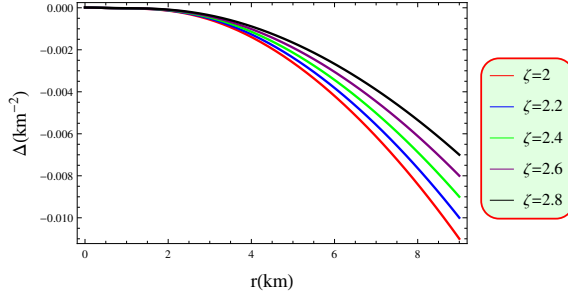


Figure 4: Plot of  $\Delta$  against  $r$ .

### 5.3 Gradients

To determine the optimal values of  $\rho$ ,  $p_r$  and  $p_t$  within the star's interior, we examine the gradients of pressure and density through plotted data. As shown in Figure 5, these gradients are uniformly negative across the star's interior. This pattern suggests that both energy density and pressure are maximized at the core and progressively diminish towards the outer layers.

### 5.4 Density and Pressure of Quark Matter

In quark matter, density is extremely high, often exceeding nuclear densities found in atomic nuclei as quarks are packed closely within a deconfined state. The pressure is likewise immense, driven by interactions between quarks and it plays a crucial role in supporting structures like neutron stars against gravitational collapse. Figure 6 shows how the  $\rho_q$  and  $p_q$ , which are influenced by quark matter, change within the star. Both values are positive for each coupling parameter  $\zeta$  given in the figure. They start high inside the star and gradually decrease towards the boundary.

### 5.5 Equation of State Parameter

In our model, the EoS parameters  $\omega_r$  and  $\omega_t$  defined by the relations  $\omega_r = \frac{p_r}{\rho}$  and  $\omega_t = \frac{p_t}{\rho}$ , respectively, must lie within the range  $(0, 1)$ . In astrophysics and cosmology, these parameters play a vital role in describing the behavior of various components in the universe. Figure 7 represents the behavior of  $\omega_r$  and  $\omega_t$ , both of which lie within this interval. This range suggests that the matter in our system is conventional, non-exotic nature.

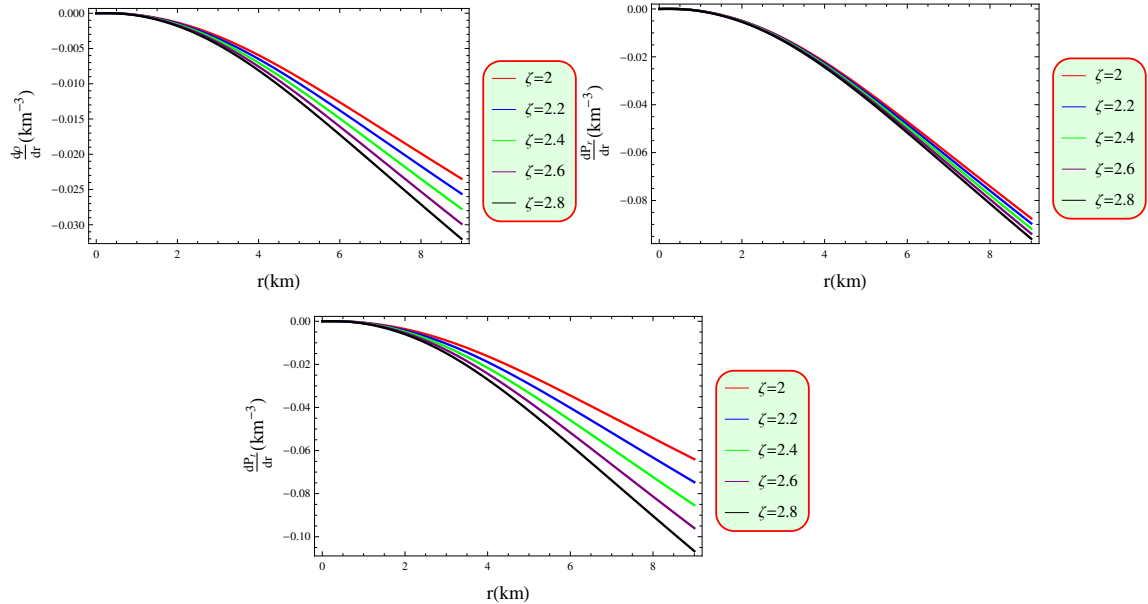


Figure 5: Plots of  $\frac{d\rho}{dr}$ ,  $\frac{dp_r}{dr}$  and  $\frac{dp_t}{dr}$  against  $r$ .

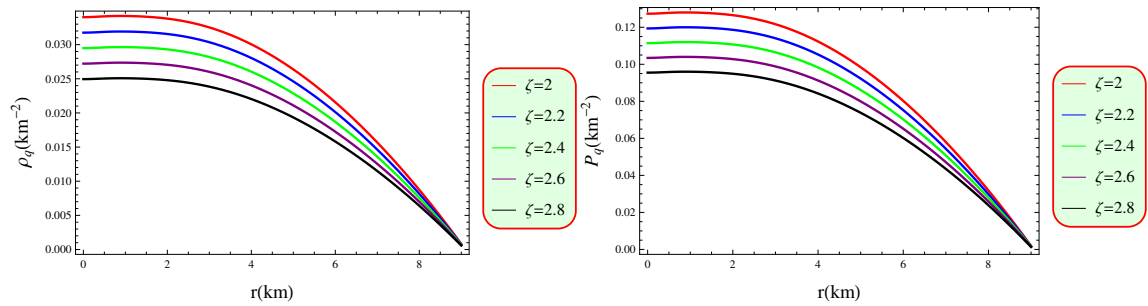


Figure 6: Plots of  $\rho_q$  and  $p_q$  against  $r$ .

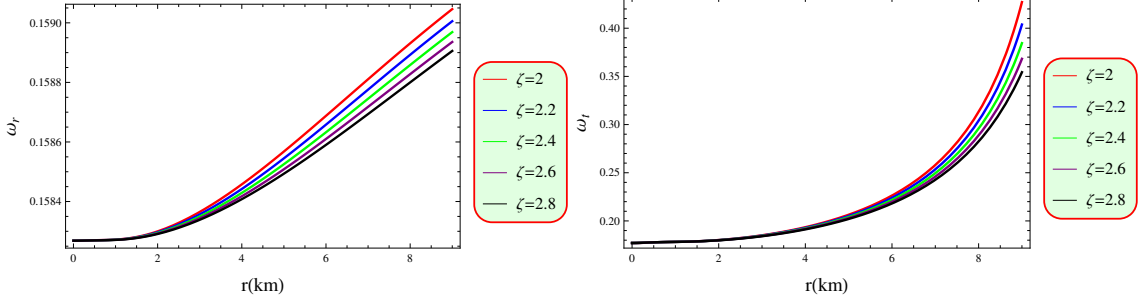


Figure 7: Graphs of EoS against  $r$ .

## 5.6 Energy Conditions

To ensure realistic matter and energy distributions, certain conditions must link energy density and pressures, especially in GR. These energy conditions help to classify matter as normal or exotic and are defined by specific mathematical inequalities.

1. Null energy condition is represented as

$$0 \leq \rho + p_r, \quad 0 \leq \rho + p_t.$$

2. Dominant energy condition is expressed as

$$0 \leq \rho - p_r, \quad 0 \leq \rho - p_t.$$

3. Weak energy condition is presented as

$$0 \leq \rho + p_r, \quad 0 \leq \rho + p_t, \quad 0 \leq \rho.$$

4. Strong energy condition is stated as

$$0 \leq \rho + p_r, \quad 0 \leq \rho + p_t, \quad 0 \leq \rho + p_r + 2p_t.$$

These inequalities are plotted in Figure 8 to check if they hold throughout the star's interior. The plots show that all these conditions are met across the entire star, confirming that the matter distribution is normal (not exotic).

## 5.7 Mass-Radius Function

The radius of the star is determined by the condition  $p(R) = 0$ . The gravitational mass ( $M(R)$ ) and baryon mass ( $M_B$ ) [72] of a compact star differ

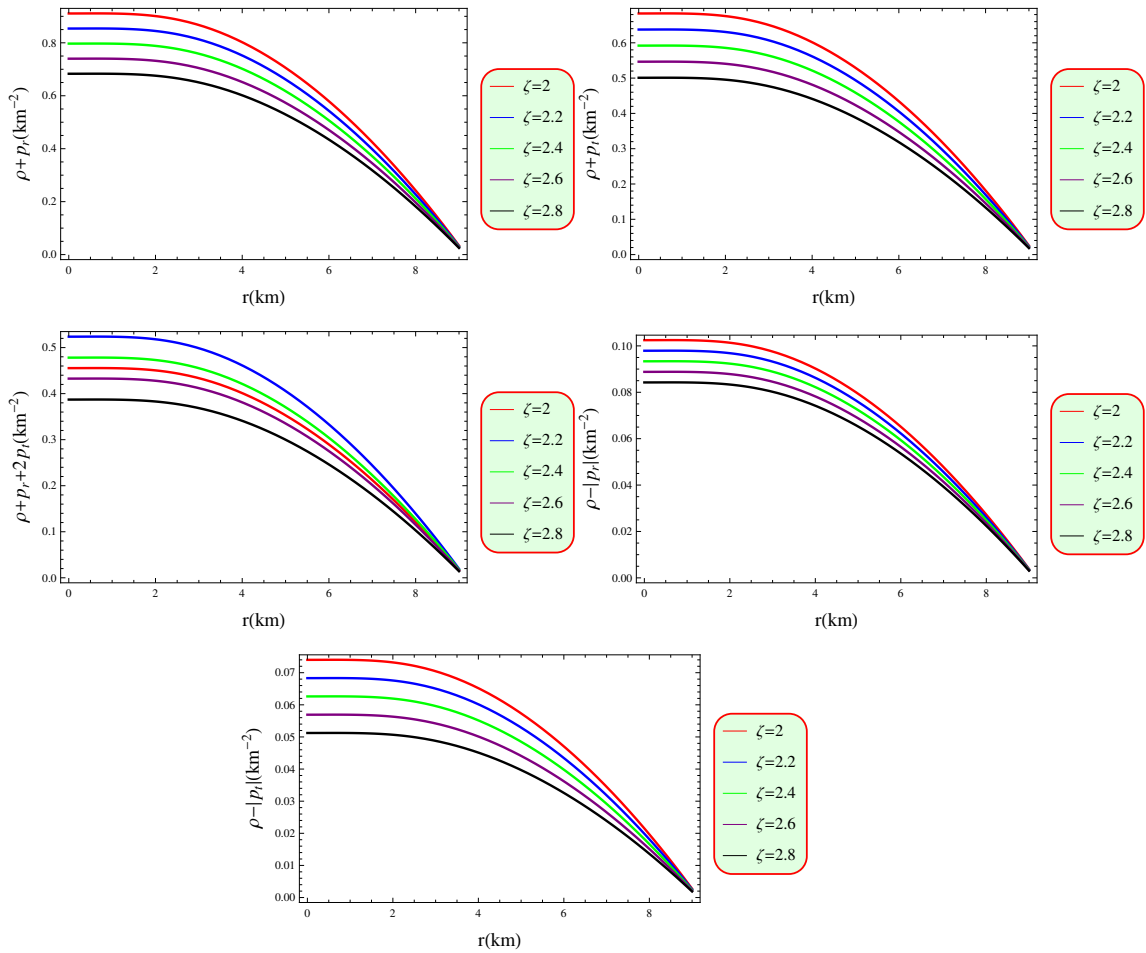


Figure 8: Graphs of energy conditions against  $r$ .

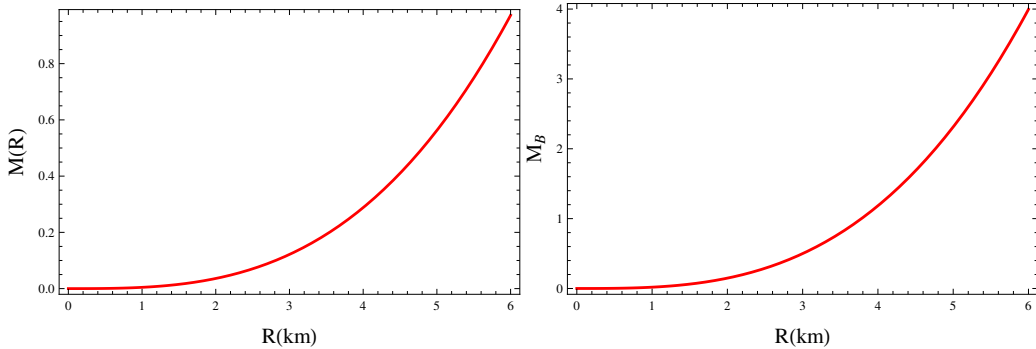


Figure 9: Plots of  $M(R)$  and  $M_B$  against  $R$ .

fundamentally in both their definitions and physical interpretations. Gravitational mass is defined as  $M = \int_0^R 4\pi r^2 \rho dr$ , where  $\rho$  represents the total energy density, including contributions from rest mass, internal energy and pressure. This mass generates the star's gravitational field and accounts for energy losses such as radiation or neutrino emissions, thus reflecting the effective mass of the star. In contrast, baryon mass is defined as  $M_B = \int_0^R 4\pi r^2 e^{\beta/2} \rho dr$ , where  $e^{\beta/2}$  is a factor that incorporates the effects of spacetime. It quantifies the total rest mass of baryonic matter, such as protons and neutrons, without considering energy losses. As a result, the baryon mass is always greater than the gravitational mass.

Figure 9 shows that both masses increase with the surface radius  $R$ . The gravitational mass typically falls within values such as 0.1, 0.2 etc., while the baryon mass is significantly higher, with values like 1, 2, 3 and so on. This difference arises because the baryon mass includes the factor  $e^{\beta/2}$ , amplifying the effects of spacetime. The distinction between these two masses is crucial for understanding the physical and gravitational properties of hybrid stars. The plotted results align with theoretical expectations, emphasizing the significant role of spacetime effects and relativistic contributions in differentiating baryonic and gravitational masses.

## 6 Stability

In this section, we examine the stability by analyzing the compactness, redshift, causality condition and Herrera cracking as well as adiabatic index.

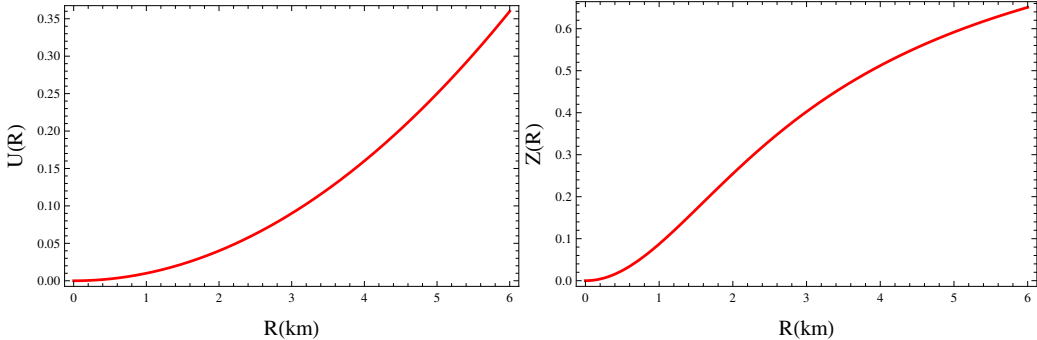


Figure 10: Plots of  $U(R)$  and  $Z(R)$  against  $R$ .

The compactness function, denoted as  $U(R) = \frac{M(R)}{R}$ , is a key parameter for assessing a star's stability. To avoid gravitational collapse, a star's compactness should stay below the threshold value of  $\frac{4}{9}$  [73]. This ensures that the gravitational pull is not strong enough to trigger collapse. Thus, maintaining  $U(R)$  below this limit is essential for a stable configuration. Figure 10 (left plot) shows that the compactness steadily increases but remains safely within the required stability range.

The redshift parameter is essential for analyzing the stability of gravastars and identifying them through their structural characteristics. For an isotropic matter distribution, the redshift typically remains below a value of 2 [74]. It can be calculated using the formula  $Z(R) = (1 - 2U(R))^{-\frac{1}{2}} - 1$ . As shown in Figure 10 (right plot), the redshift parameter consistently remains within the required limit,  $Z(R) < 2$ . Within the star, the redshift stays positive and finite, gradually increasing as it approaches the surface, thereby providing insight into the stability of our model.

The speed of sound is an important factor that must be kept within a specific range  $[0, 1]$  to ensure that the model remains stable [75]. The square of the radial and tangential sound speeds can be determined using the following expressions

$$v_r^2 = \frac{dp_r}{d\rho}, \quad v_t^2 = \frac{dp_t}{d\rho}. \quad (28)$$

According to the causality conditions, for the model to be stable within the star's interior, the following conditions must be hold:  $0 \leq v_r^2 \leq 1$  and  $0 \leq v_t^2 \leq 1$ . Additionally, the radial and tangential components of sound

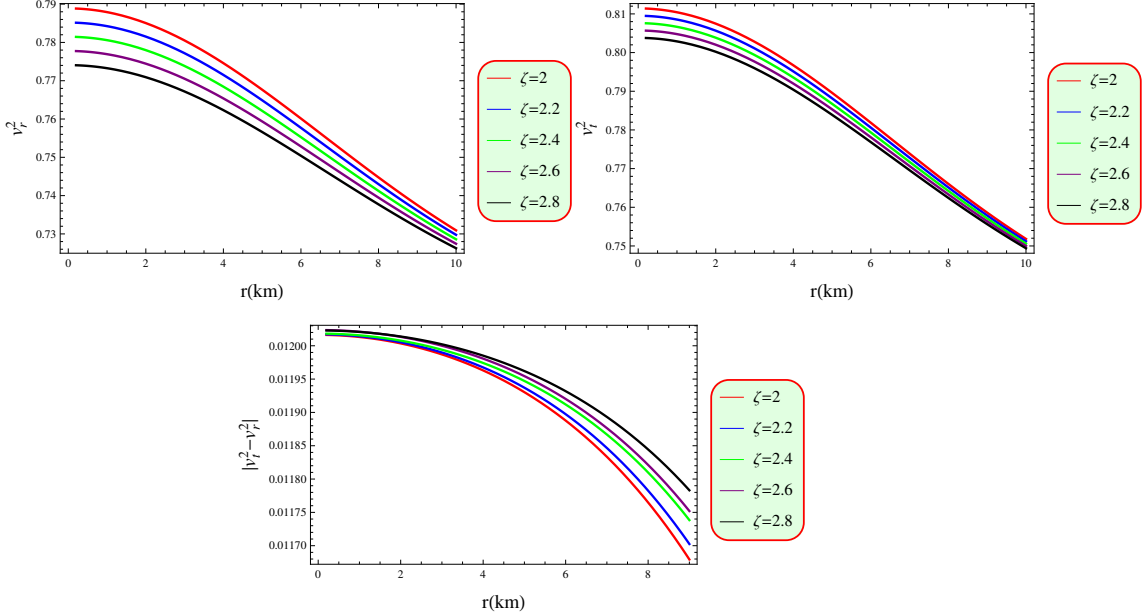


Figure 11: Plots of causality conditions and Herrera cracking against  $r$ .

speed are important in testing cracking instability, as described in criteria by Herrera [76]. The cracking condition can be expressed mathematically as  $0 \leq |v_t^2 - v_r^2| \leq 1$ . These values remain below 1 across all variations of parameter  $\zeta$  in our model. Figure 11 confirms that the model aligns with the stability conditions specified above.

The adiabatic index  $\Gamma$  is an important astrophysical parameter that indicates the stability of a fluid. The radial ( $\Gamma_r$ ) and tangential ( $\Gamma_t$ ) components of the adiabatic index are expressed as

$$\Gamma_r = \frac{v_r^2(p_r + \rho)}{p_r}, \quad \Gamma_t = \frac{v_t^2(p_t + \rho)}{p_t}.$$

In the context of compact objects,  $\Gamma_r$  and  $\Gamma_t$  must be greater than  $\frac{4}{3}$  to ensure a stable configuration, as this condition prevents collapse due to gravitational forces [77]. The adiabatic index thus plays a critical role in analyzing the stability of stellar structures and understanding the behavior of matter under extreme conditions. Figure 12 demonstrates that the system achieves stability by satisfying the required limit. This stability supports the formation of a viable hybrid star, capable of withstanding gravitational collapse and

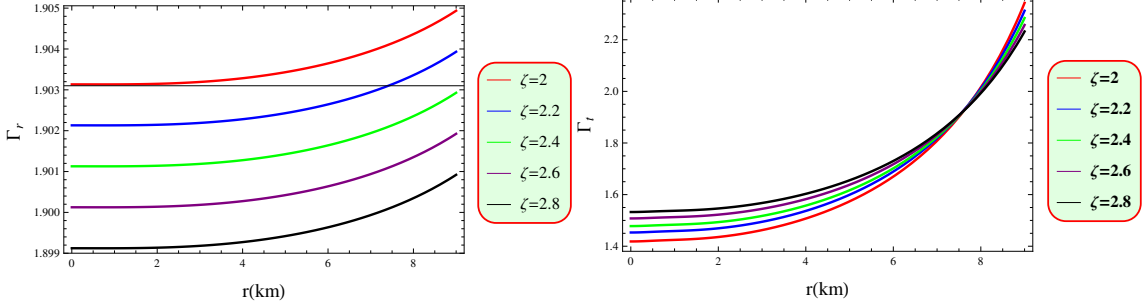


Figure 12: Plots of  $\Gamma_r$  and  $\Gamma_t$  against  $r$ .

preventing energy dissipation.

## 6.1 Equilibrium Equations

In this subsection, the Tolman-Oppenheimer-Volkoff (TOV) equation has been modified to incorporate the effects of  $f(Q)$  gravity and quark matter [78]. The equation represents the equilibrium of the total forces acting on the system, including hydrostatic, gravitational, anisotropic and quark matter contributions. This balance is expressed as

$$F_g + F_h + F_a + F_q = 0. \quad (29)$$

Here, the mathematical expressions for each force are as follows

- Gravitational Force:  $F_g = -\frac{\alpha'}{2}(\rho + p_r)$ .
- Hydrostatic Force:  $F_h = -\frac{dp_r}{dr}$ .
- Anisotropic Force:  $F_a = \frac{2}{r}(p_t - p_r)$ .
- Quark Matter Force:  $F_q = -\frac{\alpha'}{2}(\rho_q + p_q) - \frac{dp_q}{dr}$ .

The modified TOV equation is then written as

$$-\frac{\alpha'}{2}(\rho + p_r) - \frac{dp_r}{dr} + \frac{2}{r}(p_t - p_r) - \frac{\alpha'}{2}(\rho_q + p_q) - \frac{dp_q}{dr} = 0. \quad (30)$$

To ensure the model's stable equilibrium, these forces must be properly balanced. Figure 13 illustrates that stability is maintained when the sum of  $F_a$ ,  $F_g$ ,  $F_h$  and  $F_q$  is zero. This indicates that the hybrid star remains in equilibrium for various values of  $\zeta$ .

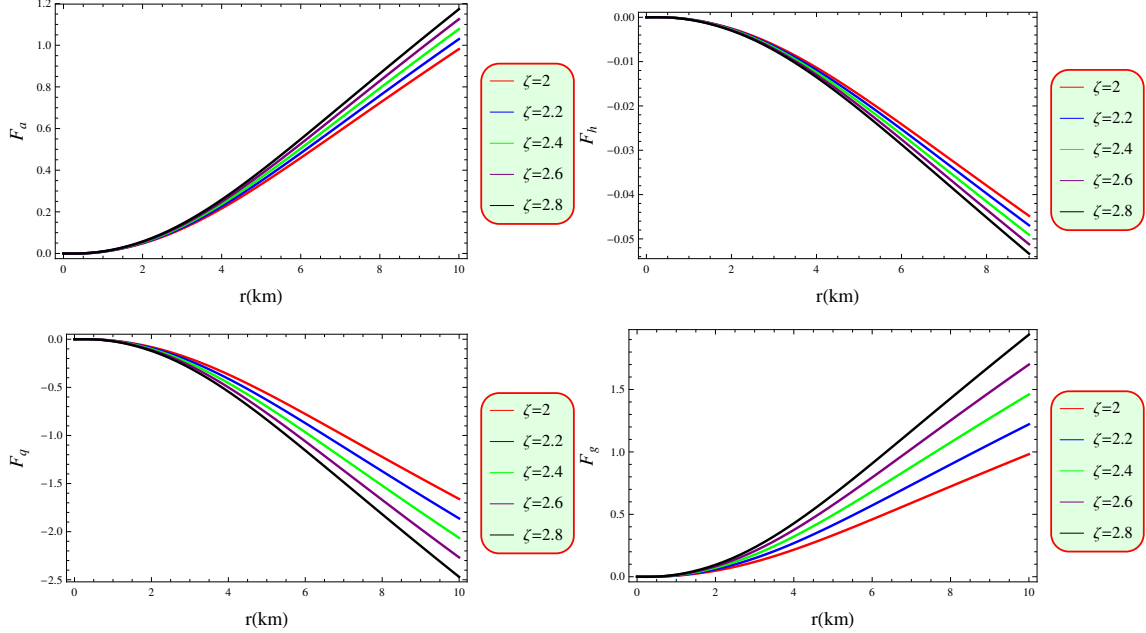


Figure 13: Graphs of TOV equation versus  $r$ .

## 6.2 Bounds of the Coupling Parameter

We now aim to determine the bounds of the coupling parameter  $\zeta$ . Using the trace energy condition,  $\rho - p_r - 2p_t > 0$ , at the star surface, we determine the following limit for  $\zeta$ . Additionally, since the transverse sound velocity inside the star must be less than 1 (i.e.,  $\frac{dp_t}{d\rho} < 1$  at the boundary), this condition also gives us another limit for  $\zeta$ . The mathematical expression can be obtained in Appendix D. By combining the two inequalities for  $\zeta$  above, we obtain a reasonable bound for  $\zeta$  as  $\Psi < \zeta < 1 + \Phi$ . The final bound ensures that the model remains physically consistent with both energy and stability conditions.

## 7 Summary and Discussion

In this paper, we have developed a model of anisotropic compact stars, specifically a hybrid star, in which strange quark matter and normal hadronic matter are combined using a two-fluid distribution. This model is free from any

mathematical or geometrical issues. We have investigated the solution of the hybrid star within the framework of  $f(Q)$  gravity, utilizing the Finch-Skea metric. For our analysis, we have selected the compact star EXO 1785-248, which serves as a strong example of a hybrid star. The key physical properties and stability of this hybrid star have been examined and are summarized as follows.

- The metric potentials are continuous and show a monotonic increase with  $r$ . This behavior reflects a smooth evolution of the spacetime structure. The absence of abrupt or sudden changes from the star's center to its boundary confirms a singularity-free and physically consistent model. The finite nature of these potentials at the core validates the theoretical framework, demonstrating a realistic stellar configuration that adheres to fundamental physical and geometric constraints. This makes the model highly suitable for describing compact stars (Figure 1).
- The physical behavior of the hybrid star model shows that  $\rho$ ,  $p_r$ ,  $p_t$ ,  $\rho_q$ , and  $p_q$  reach their maximum values at the center and gradually decrease towards the surface. This indicates a well-behaved and physically consistent solution. As the parameter  $\zeta$  increases, the density and both radial as well as transverse pressures decrease. This suggests that  $\zeta$  has a significant impact on the star's internal structure, potentially influencing its overall equilibrium and matter distribution (Figures 2 and 6).
- We have noticed that radial and transverse pressures change in a way that closely follows a linear pattern with density, and this happens for all values of  $\zeta$ . This shows that the pressures adjust smoothly, helping the star to maintain a proper balance in its structure. If the pressures were uneven, the star might either collapse or become too spread out (Figure 3).
- We have analyzed that the anisotropic factor is negative which satisfies the condition  $p_t < p_r$ . This means that the force from anisotropy combines with the gravitational force to help to compress the star (Figure 4).
- It is found that the gradients of  $\rho$ ,  $p_r$ , and  $p_t$  are negative throughout the star interior. This confirms that these quantities are the highest

at the core of the star. As a result, the negative gradients support a stronger gravitational pull, helping the star to compress further (Figure 5).

- The EoS parameter between 0 and 1 indicates a consistent relationship between pressure and energy density. This confirms that the hybrid star meets the required physical conditions (Figure 7).
- All energy conditions have positive results, showing that the energy density and pressures follow acceptable physical limits. This confirms the presence of hadronic matter in the hybrid star (Figure 8).
- The behavior of the mass function shows an increasing trend as the radial coordinate increases and the mass distribution shows a physically possible and realistic behavior for the hybrid star (Figure 9).
- We have also checked the stability of the gravastar by examining compactness, redshift, causality conditions and the adiabatic index. Our findings confirm that the stability limits support the existence of a stable hybrid star (Figure 10-12).
- We have observed that  $F_a$  and  $F_g$  have positive values, whereas  $F_q$  and  $F_h$  are negative. Since the total force balance is zero, the system stays in equilibrium within this framework (Figure 13).

It is worth mentioning that compact stars such as neutron stars, usually rotate and possess angular momentum. Therefore, a fully spherically symmetric solution may not always be applicable. However, for simplicity, this paper focuses on non-rotating compact stars, excluding angular momentum. Previous studies in  $f(Q)$  gravity have similarly analyzed non-rotating compact stars [79]. Within the framework of  $f(Q)$  gravity, we have explored the Finch-Skea metric using two fluid distributions: strange quark matter and hadronic matter. Our analysis of a compact star candidate in  $f(Q)$  gravity has demonstrated the viability of addressing both central singularity and stability conditions for the internal fluid distribution. This led us to conclude that such a dense, compact object made of quark matter could serve as the excellent model for hybrid stars, allowing the investigation of their physical properties on both theoretical and astrophysical scales. Furthermore, we note that, beyond the conventional GR approach, other higher-order gravity

theories can also be employed to explore these physical characteristics under specific constraints.

In contrast,  $f(Q)$  gravity [79] incorporates non-metricity  $Q$  as a fundamental component of gravity, making it uniquely suited to model environments where anisotropic pressures and non-singular configurations exist. The theory provides a more flexible approach for handling the internal structure of hybrid stars, which often involve extreme densities and complex phase transitions between quark and hadronic matter. Studies have shown that  $f(Q)$  gravity can support supermassive hybrid stars and explain the observed mass-radius relationships for compact stars more effectively than  $f(R)$  and  $f(\mathcal{T})$ . Moreover,  $f(Q)$  gravity offers non-singular solutions that can accommodate exotic matter states without the singularities typically associated with  $f(R)$  gravity. This flexibility is crucial for modeling hybrid stars, where the internal pressure distribution can vary significantly. This capacity to model smooth, continuous solutions is essential for understanding the complex internal structures of these stars.

While  $f(Q)$  gravity is a relatively new theory with limited empirical validation compared to well-established frameworks like  $f(R)$ , initial results have shown promising potential, particularly in the modeling of non-singular hybrid stars and the handling of anisotropic pressures. Comparative studies with  $f(R)$  and  $f(\mathcal{T})$  are essential to fully explore the capabilities of  $f(Q)$  and identify areas where it could be further refined. As research progresses,  $f(Q)$  gravity has the potential to become a viable alternative to  $f(R)$ , offering new insights into the structure of compact stars and other astrophysical phenomena.

We have found that the  $f(Q)$  theory is highly flexible in modeling gravitational interactions, particularly in environments characterized by anisotropic pressures and non-singular configurations. Bhar et al. [80] employed the Krori-Barua metric to model hybrid stars within the framework of  $f(Q)$  gravity, while we adopted the Finch-Skea metric, which offers a more flexible and realistic representation of compact stars, especially in evaluating stability. Quantitatively, our Herrera cracking graph exhibited a monotonic decrease across the stellar interior, indicating smooth and stable behavior throughout. In contrast, the analysis [80] showed a cracking profile that initially increased and then decreased, suggesting fluctuating stability and possible local instabilities. Our model also satisfies the condition  $\Gamma > \frac{4}{3}$  for the adiabatic index at all radii, ensuring dynamical stability, whereas this index in [80] varied and dropped below this threshold in certain regions. The maximum com-

pactness factor in our configuration reaches  $U(R) = 0.192$ , remaining well within the Buchdahl limit, while the corresponding values in [80] appeared higher and more variable. Additionally, the surface redshift in our case attains a maximum of  $Z(R) = 0.275$ , comfortably within the theoretical bound, in contrast to the results [80], which approached or in some cases exceeded this limit. These distinctions illustrated that the Finch-Skea metric yield a more consistent stable and physically viable configuration compared to the Krori-Barua metric, particularly with respect to the Herrera cracking, sound speed criteria and adiabatic behavior. Our results align well with the previous studies in  $f(R)$  [81] and  $f(\mathcal{T})$  [10] theories of gravity. We can conclude that our study provides a comprehensive and stable hybrid star solution in  $f(Q)$  gravity, offering enhanced insights into the stability analysis.

## Appendix A: Non-Metricity Scalar and Superpotential Representation

The non-metricity scalar is defined by

$$Q = -g^{\gamma\psi}(\mathbb{L}_{\nu\gamma}^\mu \mathbb{L}_{\psi\mu}^\nu - \mathbb{L}_{\nu\mu}^\mu \mathbb{L}_{\gamma\psi}^\nu). \quad (\text{A1})$$

Here, the Levi-Civita connection is represented by the deformation tensor as  $\Gamma_{\nu\varsigma}^\mu = -\mathbb{L}_{\nu\varsigma}^\mu$ , where

$$\mathbb{L}_{\nu\varsigma}^\mu = -\frac{1}{2}g^{\mu\lambda}(\nabla_\varsigma g_{\nu\lambda} + \nabla_\nu g_{\lambda\varsigma} - \nabla_\lambda g_{\nu\varsigma}). \quad (\text{A2})$$

The superpotential is expressed as

$$\mathbb{P}^{\mu\psi\gamma} = \frac{1}{4}[Q^{\psi\mu\gamma} - Q^{\mu\psi\gamma} + Q^{\psi\mu\gamma} + Q^{\gamma\mu\psi} - \tilde{Q}_\mu g^{\psi\gamma} + Q^\mu g^{\psi\gamma}], \quad (\text{A3})$$

where

$$Q_\mu = Q_{\mu\psi}^\psi, \quad \tilde{Q}_\mu = Q_{\mu\psi}^\psi.$$

Thus,  $Q$  can be further rewritten as [82]

$$Q = -Q_{\mu\gamma\psi} \mathbb{P}^{\mu\gamma\psi} = -\frac{1}{4}(-Q^{\mu\psi\rho} Q_{\mu\psi\rho} + 2Q^{\mu\psi\rho} Q_{\rho\mu\psi} - 2Q^\rho \tilde{Q}_\rho + Q^\rho Q_\rho). \quad (\text{A4})$$

## Appendix B: Matter Variables and Quark Matter

The expressions for the matter density and pressures associated with regular hadronic matter are as follows

$$\begin{aligned}
\rho &= \left[ 4\xi r^{11} \varphi \chi^5 (4\mathcal{B}_g \kappa + 36\zeta \chi + 3h\kappa - 42) + 8\xi r^9 \varphi \chi^4 (8\mathcal{B}_g \kappa + 30\zeta \chi + 6h\kappa \right. \\
&\quad + 4\chi - 27) + 4\xi r^7 \varphi \chi^3 (24\mathcal{B}_g \kappa + \chi(6\zeta(4 - 5\chi) + 13) + 18h\kappa - 30) - 8\xi \\
&\quad \times r^5 \varphi \chi^2 (-8\mathcal{B}_g \kappa + 2\chi(9\zeta \chi + 1) - 6h\kappa + 3) + 4\varphi \chi (4\mathcal{B}_g \kappa + \chi(8\zeta \chi - 15) \\
&\quad + 3h\kappa) \xi r^3 + 4(r^2 \chi)^{3/2} (16\mathcal{B}_g \kappa \xi^2 + \chi(\xi^2(5 - 16\zeta \chi) + 24\zeta \varphi^2) + 12h\kappa \xi^2 \\
&\quad - 3\varphi^2) + r^2 (r^2 \chi)^{3/2} (4\mathcal{B}_g \kappa (24\xi^2 \chi + \varphi^2) - (4\xi^2(\chi(\zeta \chi - 5) + 3) + 5\varphi^2 \\
&\quad \times (3 - 20\zeta \chi)) 2\chi + 3h\kappa (24\xi^2 \chi + \varphi^2)) + r^2 (r^2 \chi)^{5/2} (4\xi^2 \chi (16\mathcal{B}_g \kappa + 12\zeta \\
&\quad \times \chi + 12h\kappa + 5\chi - 18) + \varphi^2 (16\mathcal{B}_g \kappa + \chi(\zeta(\chi + 2) - 13) + 12h\kappa - 12)) \\
&\quad - 4\kappa \xi^2 (4\mathcal{B}_g + 3h) \sqrt{r^2 \chi} + r^{12} \varphi^2 \chi^5 \sqrt{r^2 \chi} (4\mathcal{B}_g \kappa + 108\zeta \chi + 3h\kappa - 66) + r \\
&\quad \times \chi^3 (r^2 \chi)^{3/2} (\varphi^2 (16\mathcal{B}_g \kappa + 252\zeta \chi + 12h\kappa + 11\chi - 90) - 24\xi^2 \chi) + 2r^8 \chi^3 \\
&\quad \times \sqrt{r^2 \chi} (2\xi^2 \chi (4\mathcal{B}_g \kappa + 3(4\zeta \chi + h\kappa - 6)) + \varphi^2 (12\mathcal{B}_g \kappa + \chi(-33\zeta \chi + 96\zeta \\
&\quad + 8) + 9h\kappa - 27)) - 48\xi r^{13} \varphi \chi^6 - 18r^{14} \varphi^2 \chi^6 \sqrt{r^2 \chi} - 24\xi r \varphi \chi \Big] \Big[ (3s - 1) \right. \\
&\quad \times \left. \kappa \sqrt{r^2 \chi} (r^2 \chi + 1)^4 (2\xi + r\varphi \sqrt{r^2 \chi})^2 \right]^{-1}, \tag{B1} \\
p_r &= \left[ \sqrt{r^2 \chi} (h\kappa (240r^2 \xi^4 \varphi^2 (r^2 \chi)^{3/2} + 60r^4 \xi^2 \varphi^4 (r^2 \chi)^{5/2} + 64\xi^6 \sqrt{r^2 \chi} + r^{12} \right. \\
&\quad \times \varphi^6 \chi^3 \sqrt{r^2 \chi} + 12r^{11} \xi \varphi^5 \chi^3 + 160r^7 \xi^3 \varphi^3 \chi^2 + 192r^3 \xi^5 \varphi \chi) (\chi r^2 + 1)^4 + s \\
&\quad \times (-64\xi^4 (-16\mathcal{B}_g \kappa \xi^2 + \chi(16\zeta \chi - 5) \xi^2 + 3\varphi^2(5 - 8\zeta \chi)) (r^2 \chi)^{3/2} - 32 \\
&\quad \times r^2 \xi^4 (\chi(4(\chi(\zeta \chi - 5) + 3) \xi^2 + 3\varphi^2(25 - 44\zeta \chi)) - 6\mathcal{B}_g \kappa (8\chi \xi^2 + 5\varphi^2)) \\
&\quad \times (r^2 \chi)^{3/2} + 16r^2 \xi^2 (4\chi (16\mathcal{B}_g \kappa + 12\zeta \chi + 5\chi - 18) \xi^4 + 3\varphi^2 \xi^2 (80\mathcal{B}_g \kappa + \chi \\
&\quad \times (8\zeta(2 - 15\chi) - 5) - 20) + 6\varphi^4 (24\zeta \chi - 5)) (r^2 \chi)^{5/2} + 16r^4 \xi^2 (\mathcal{B}_g \kappa (16 \\
&\quad \times \chi^2 \xi^4 + 360\varphi^2 \chi \xi^2 + 15\varphi^4) + \chi (24\chi (2\zeta \chi - 3) \xi^4 - 6\varphi^2 \xi^2 (\chi (53\chi \zeta - 64\zeta \\
&\quad - 30) + 55) + \varphi^4 (316\zeta \chi - 75))) (r^2 \chi)^{5/2} - 4r^4 (96\chi^2 \xi^6 - 12\varphi^2 \chi (80\mathcal{B}_g \kappa \\
&\quad + 268\zeta \chi + 35\chi - 210) \xi^4 + \varphi^4 (-240\mathcal{B}_g \kappa + \chi (32\zeta (5\chi - 9) + 105) + 120) \right]
\end{aligned}$$

$$\begin{aligned}
& \times \xi^2 + 3\varphi^6(1 - 8\zeta\chi) \left( r^2\chi \right)^{7/2} - 18r^{22}\varphi^6\chi^8\sqrt{r^2\chi} + 256\mathcal{B}_g\kappa\xi^6\sqrt{r^2\chi} + 2 \\
& \times r^{20}\varphi^6\chi^7(2\mathcal{B}_g\kappa + 54\zeta\chi - 33)\sqrt{r^2\chi} + r^{18}\varphi^4\chi^6(\varphi^2(16\mathcal{B}_g\kappa + 252\zeta\chi + 11 \\
& \times \chi - 90) - \xi^2\chi)\sqrt{r^2\chi} + 2r^{16}\varphi^4\chi^5(12\chi(10\mathcal{B}_g\kappa + 158\zeta\chi - 125)\xi^2 + (12 \\
& \times \mathcal{B}_g\kappa + \chi(-33\chi\zeta + 96\zeta + 8) - 27)\varphi^2)\sqrt{r^2\chi} + r^{14}\varphi^2\chi^4(2400\chi^2\xi^4 + 12 \\
& \times \varphi^2\chi(80\mathcal{B}_g\kappa + 68\zeta\chi + 45\chi - 330)\xi^2 + \varphi^4(16\mathcal{B}_g\kappa + \chi(24\zeta(\chi + 2) - 13) \\
& - 12))\sqrt{r^2\chi} + 2r^{12}\varphi^2\chi^3(2\mathcal{B}_g\kappa(240\chi^2\xi^4 + 360\varphi^2\chi\xi^2 + \varphi^4) + \chi(48\chi(78\zeta \\
& - 85)\xi^4 + 4\varphi^2(\chi(105 - 319\chi\zeta + 672\zeta) - 285)\xi^2 + \varphi^4(20\zeta\chi - 3))\sqrt{r^2\chi} \\
& - 192r^{21}\xi\varphi^5\chi^8 - 384r\xi^5\varphi\chi + 24r^{19}\xi\varphi^5\chi^7(2\mathcal{B}_g\kappa + 42\zeta\chi - 29) + r^3\xi^5\varphi\chi \\
& \times (12\mathcal{B}_g\kappa + \chi(8\zeta\chi - 15)) + 24r^{17}\xi\varphi^3\chi^6(\varphi^2(\mathcal{B}_g\kappa + 94\zeta\chi + 5\chi - 39) - \xi^2 \\
& \times \chi 80) + 64r^5\xi^3\varphi\chi^2((-68\zeta\chi^2 + 6\chi + 48\mathcal{B}_g\kappa - 6)\xi^2 + 3\varphi^2(16\zeta\chi - 5)) \\
& + 8r^9\xi\varphi\chi^3(48\chi(8\mathcal{B}_g\kappa + 14\zeta\chi + 3\chi - 15)\xi^4 + 8\varphi^2(40\mathcal{B}_g\kappa - 2\chi(25\chi\zeta + 5 \\
& - 12\zeta) - 15)\xi^2 + 3\varphi^4(32\zeta\chi - 5)) + 4r^{15}\xi\chi^5(16\chi(10\mathcal{B}_g\kappa + 114\zeta\chi - 105) \\
& \times \varphi^3\xi^2 + 3\varphi^2(24\mathcal{B}_g\kappa + \chi(-54\chi\zeta + 136\zeta + 15) - 46)) + 8r^{13}\xi\varphi\chi^4(192\chi \\
& \times \xi^4 + 8(40\mathcal{B}_g\kappa + 222\zeta\chi + 20\chi - 135)\varphi^2\chi\xi^2 + 3\varphi^4(8\mathcal{B}_g\kappa + \chi(2\zeta(\chi + 8 \\
& - 5) - 5)) + 4r^{11}\xi\chi^3(12\mathcal{B}_g\kappa\varphi(16\chi^2\xi^4 + 80\varphi^2\chi\xi^2 + \varphi^4) + \chi\varphi^5(3(136\zeta\chi \\
& - 25) - 8\xi^2(\chi(58\chi\zeta - 264\zeta - 65) + 150)\varphi^3 + \xi^4\chi(10\zeta\chi - 13)\varphi)) + 32 \\
& \times r^7\xi^3\varphi\chi^2(4\mathcal{B}_g\kappa(36\chi\xi^2 + 5\varphi^2) + \chi((2\chi(24\zeta - 34\zeta\chi + 33) - 84)\xi^2 + \varphi^2 \\
& \times (224\zeta\chi - 75))))\Bigg] \Bigg[ \kappa(3s - 1)(\chi r^2 + 1)^4(6r^2\xi\varphi^2(r^2\chi)^{3/2} + 8\xi^3\sqrt{r^2\chi} \\
& + r^7\varphi^3\chi^2 + 12r^3\xi^2\varphi\chi)^2 \Bigg]^{-1}, \tag{B2}
\end{aligned}$$

$$\begin{aligned}
p_t = & \Bigg[ r(\chi r^2 + 1)(r^3\varphi^3(\chi(\chi r^4 + (2 - 12\zeta\chi)r^2 - 8\zeta) + 1)(r^2\chi)^{3/2} + 4r\xi^2\varphi \\
& \times (\chi(3\chi r^4 + (6 - 20\zeta\chi)r^2 - 8\zeta) + 3)\sqrt{r^2\chi} + 8\xi^3(\chi(\chi r^2 - 4\zeta\chi + 2)r^2 \\
& + 1) + 2r^4\xi\varphi^2\chi(\chi(3\chi r^4 + (6 - 28\zeta\chi)r^2 - 16\zeta) + 3)) \Big( [2\left(\frac{\varphi\chi r^2}{2\sqrt{r^2\chi}} + \frac{1}{2}\right. \\
& \times \varphi\sqrt{r^2\chi}\Big) \Big[ \xi + \frac{1}{2}r\varphi\sqrt{r^2\chi} \Big]^{-1} \Big)^2 + \Big[ 4(-42r^8\zeta\varphi^3\chi^4(r^2\chi)^{3/2} + 60r^8s\zeta \\
& \times \varphi^3\chi^4(r^2\chi)^{3/2} + 112r^8\zeta\xi^2\varphi\chi^4(r^2\chi)^{3/2} - 4r^2\varphi^3(r^2\chi)^{3/2} + 10(r^2\chi)^{3/2} \\
& \times r^8\varphi^3\chi^3 - 14r^8s\varphi^3\chi^3(r^2\chi)^{3/2} + 64r^8\zeta\varphi^3\chi^3(r^2\chi)^{3/2} - 136(r^2\chi)^{3/2}r^8
\end{aligned}$$

$$\begin{aligned}
& \times \xi^2 \varphi \chi^3 - 16r^2 \xi^2 \varphi (r^2 \chi)^{3/2} + 48s \xi^2 \varphi (r^2 \chi)^{3/2} - 56 \xi^2 \varphi (r^2 \chi)^{3/2} - s \zeta \\
& \times \xi^2 \varphi \chi 2(r^2 \chi)^{3/2} + 64\zeta \xi^2 \varphi \chi (r^2 \chi)^{3/2} - 4r^4 \varphi^3 (r^2 \chi)^{5/2} - 6r^2 \varphi^3 (r^2 \chi)^{5/2} \\
& - 12r^2 s \varphi^3 (r^2 \chi)^{5/2} + 32\zeta \varphi^3 (r^2 \chi)^{5/2} - 8r^2 \xi^2 \varphi (r^2 \chi)^{5/2} - 6s \xi^2 \varphi (r^2 \chi)^{5/2} \\
& + 16\xi^2 \varphi (r^2 \chi)^{5/2} - 18r^4 \varphi^3 (r^2 \chi)^{7/2} - 6r^{16} \varphi^3 \chi^6 \sqrt{r^2 \chi} + 36\varphi^3 \chi^6 \sqrt{r^2 \chi} \zeta \\
& \times r^{14} - 22r^{14} \varphi^3 \chi^5 \sqrt{r^2 \chi} + 4r^{12} \varphi^3 \chi^5 \sqrt{r^2 \chi} - r^{12} s \varphi^3 \chi^5 \sqrt{r^2 \chi} + 84r^{12} \zeta \\
& \times \varphi^3 \chi^5 \sqrt{r^2 \chi} - 40r^{12} \xi^2 \varphi \chi^5 \sqrt{r^2 \chi} - 30r^{12} \varphi^3 \chi^4 \sqrt{r^2 \chi} - 120\varphi^3 \chi^4 \sqrt{r^2 \chi} \\
& \times r^8 \zeta + 384r^8 s \zeta \varphi^3 \chi^4 \sqrt{r^2 \chi} + 32r^8 \xi^2 \varphi \chi^4 \sqrt{r^2 \chi} - 12r^8 s \xi^2 \varphi \chi^4 \sqrt{r^2 \chi} \\
& + 176r^8 \zeta \xi^2 \varphi \chi^4 \sqrt{r^2 \chi} - 152r^6 \zeta \xi^2 \varphi \chi^4 \sqrt{r^2 \chi} + 208r^6 s \zeta \xi^2 \varphi \chi^4 \sqrt{r^2 \chi} + 4 \\
& \times r^8 \varphi^3 \chi^3 \sqrt{r^2 \chi} - 25r^8 s \varphi^3 \chi^3 \sqrt{r^2 \chi} + 16r^8 \zeta \varphi^3 \chi^3 \sqrt{r^2 \chi} + 8r^6 \chi^3 \sqrt{r^2 \chi} \zeta \\
& \times \varphi^3 + 176r^6 s \zeta \varphi^3 \chi^3 \sqrt{r^2 \chi} - 168r^8 \xi^2 \varphi \chi^3 \sqrt{r^2 \chi} + 72r^6 \xi^2 \varphi \chi^3 \sqrt{r^2 \chi} - s \\
& \times 72r^6 \xi^2 \varphi \chi^3 \sqrt{r^2 \chi} + 64r^6 \zeta \xi^2 \varphi \chi^3 \sqrt{r^2 \chi} - 416r^4 \zeta \xi^2 \varphi \chi^3 \sqrt{r^2 \chi} + 896r^4 s \\
& \times \zeta \xi^2 \varphi \chi^3 \sqrt{r^2 \chi} + 48s \xi^2 \varphi \sqrt{r^2 \chi} - 32\xi^2 \varphi \sqrt{r^2 \chi} - 28r^{15} \xi \varphi^2 \chi^6 + 16r \xi^3 \chi \\
& \times (1 - 3s) + 20r^{13} \xi \varphi^2 \chi^5 (6\zeta \chi - 5) + h\kappa r (\chi r^2 + 1)^4 (r^3 \varphi^3 (r^2 \chi)^{3/2} + r \\
& \times 12\xi^2 \varphi \sqrt{r^2 \chi} + 8\xi^3 + 6r^4 \xi \varphi^2 \chi) + 4\mathcal{B}_g \kappa r s (\chi r^2 + 1)^4 (r^3 \varphi^3 (r^2 \chi)^{3/2} \\
& + 12r \xi^2 \varphi \sqrt{r^2 \chi} + 8\xi^3 + 6r^4 \xi \varphi^2 \chi) + 8r^3 \xi \chi (\chi \xi^2 (-13s + 16(2s - 1)\zeta \chi \\
& - 6) + 3\varphi^2 (-16\zeta \chi s + s + 8\zeta \chi - 1)) - 2r^{11} \xi \chi^4 (8\chi \xi^2 + \varphi^2 ((3s - 124\zeta \\
& - 10)\chi + 66)) + 4r^5 \xi \chi^2 (4(\chi (-4s + (2s - 1)\zeta \chi + 3) - 1)\xi^2 + \varphi^2 (120 \\
& \times \zeta \chi s + 3s + 76\zeta \chi - 11)) + 2r^7 \xi \chi^2 (\varphi^2 (\chi (-27s + 16\zeta + 48(8s - 3)\zeta \\
& \times \chi + 2) - 8) - 4\xi^2 \chi ((s - 4\zeta - 2)\chi + 6)) + 4r^9 \xi \chi^3 (4\chi (2\zeta \chi - 3)\xi^2 \\
& + \varphi^2 (\chi (-39\chi \zeta + 40\zeta + 6s(9\zeta \chi - 2) + 11) - 19))) \Big] [3s - 1]^{-1} \Big] [4\kappa r \\
& \times (\chi r^2 + 1)^4 (2\xi + r\varphi \sqrt{r^2 \chi})^3 \Big]^{-1}. \tag{B3}
\end{aligned}$$

The expressions for  $\rho_q$  and  $p_q$  are derived as follows

$$\begin{aligned}
\rho_q = & - \Big[ 4\xi r^{11} \varphi \chi^5 (4\mathcal{B}_g \kappa + 36\zeta \chi + 3h\kappa - 42) + 4\xi r^9 \varphi \chi^4 (16\mathcal{B}_g \kappa + 12h\kappa + \chi \\
& \times (6\zeta - 3s + 9) - 54) + 12\xi r^7 \varphi \chi^3 (8\mathcal{B}_g \kappa + 6h\kappa + \chi (8\zeta + 6\zeta(s - 2)\chi - s \\
& \times 5 + 6) - 10) + 4\xi r^5 \varphi \chi^2 (16\mathcal{B}_g \kappa + 3(4h\kappa + \chi (4\zeta(s - 7)\chi - s + 1) - 2)) \\
& + 4\xi r^3 \varphi \chi (4\mathcal{B}_g \kappa + 3h\kappa + 3\chi (4\zeta(5s - 1)\chi - 3s - 4)) + 4(r^2 \chi)^{3/2} (16\mathcal{B}_g \kappa
\end{aligned}$$

$$\begin{aligned}
& \times \xi^2 + 3(\varphi^2(8\zeta\chi - 1) + 4h\kappa\xi^2 + \xi^2\chi(4\zeta(s-3)\chi - s+4)) + r^2(r^2\chi)^{3/2} \\
& \times (4\mathcal{B}_g\kappa(24\xi^2\chi + \varphi^2) + 3(h\kappa(24\xi^2\chi + \varphi^2) - \chi(4\xi^2(\chi(2\zeta s\chi + 5s-5) \\
& + 2) + \varphi^2(3(s+3) - 8\zeta(4s+7)\chi))) + r^2(r^2\chi)^{5/2}(4\xi^2\chi(16\mathcal{B}_g\kappa + 3(4h \\
& \times \kappa + \chi(4\zeta - s+2) - 6)) + \varphi^2(16\mathcal{B}_g\kappa + 3(4h\kappa + \chi(16\zeta + 12\zeta(5s-1)\chi \\
& - 7s-2) - 4)) + 4\xi^2\sqrt{r^2\chi}(4\mathcal{B}_g\kappa + 3(h\kappa - 3s\chi + \chi)) + r^{12}\varphi^2\chi^5\sqrt{r^2\chi} \\
& \times (4\mathcal{B}_g\kappa + 108\zeta\chi + 3h\kappa - 66) + r^8\chi^3(r^2\chi)^{3/2}(\varphi^2(4\kappa(4B+3h) - 3\chi(s \\
& - 84\zeta - 4) - 90) - 24\xi^2\chi) + r^8\chi^3\sqrt{r^2\chi}(4\xi^2\chi(4\mathcal{B}_g\kappa + 3(4\zeta\chi + h\kappa - 6)) \\
& + 3\varphi^2(8\mathcal{B}_g\kappa + 6h\kappa + \chi(64\zeta + 6\zeta(s-4)\chi - 5s+7) - 18)) - 48\xi r^{13}\varphi\chi^6 \\
& - 18r^{14}\varphi^2\chi^6\sqrt{r^2\chi} - 24\xi r\varphi\chi\Big] \Big[ \kappa(3s-1)(r^2\chi+1)^4(4\xi r^3\varphi\chi + 4\xi^2\sqrt{r^2\chi} \\
& + r^2\varphi^2(r^2\chi)^{3/2}) \Big]^{-1}, \tag{B4}
\end{aligned}$$

$$\begin{aligned}
p_q = & \Bigg[ r\chi \Big( 144r^8\zeta\xi\varphi^3\chi^4(r^2\chi)^{3/2} - 48r^8s\zeta\xi\varphi^3\chi^4(r^2\chi)^{3/2} - r^8\xi^3\varphi\chi^4(r^2\chi)^{3/2} \\
& \times 256\zeta + 24r^2\xi\varphi^3(r^2\chi)^{3/2} - 52r^8\xi\varphi^3\chi^3(r^2\chi)^{3/2} + 40r^8s\xi\varphi^3\chi^3(r^2\chi)^{3/2} \\
& - 288r^8\zeta\xi\varphi^3\chi^3(r^2\chi)^{3/2} + 320r^8\xi^3\varphi\chi^3(r^2\chi)^{3/2} + 32r^2\xi^3\varphi(r^2\chi)^{3/2} + 96 \\
& \times s\xi^3\varphi(r^2\chi)^{3/2} + 48\xi^3\varphi(r^2\chi)^{3/2} - 320s\zeta\xi^3\varphi\chi(r^2\chi)^{3/2} + \xi^3\varphi\chi(r^2\chi)^{3/2} \\
& \times 64\zeta + 24r^4\xi\varphi^3(r^2\chi)^{5/2} + 52r^2\xi\varphi^3(r^2\chi)^{5/2} + 24r^2s\xi\varphi^3(r^2\chi)^{5/2} - 12 \\
& \times \zeta\xi\varphi^3(r^2\chi)^{5/2} + 192r^2\xi^3\varphi(r^2\chi)^{5/2} + 24s\xi^3\varphi(r^2\chi)^{5/2} - 80\xi^3\varphi(r^2\chi)^{5/2} \\
& + 112r^4\xi\varphi^3(r^2\chi)^{7/2} + 40r^{16}\xi\varphi^3\chi^6\sqrt{r^2\chi} - 192r^{14}\zeta\xi\varphi^3\chi^6\sqrt{r^2\chi} + 144\xi \\
& \times r^{14}\varphi^3\chi^5\sqrt{r^2\chi} - 28r^{12}\xi\varphi^3\chi^5\sqrt{r^2\chi} + 8r^{12}s\xi\varphi^3\chi^5\sqrt{r^2\chi} - 416r^{12}\zeta\xi\varphi^3 \\
& \times \chi^5\sqrt{r^2\chi} + 96r^{12}\xi^3\varphi\chi^5\sqrt{r^2\chi} + 192r^{12}\xi\varphi^3\chi^4\sqrt{r^2\chi} + 160r^8\zeta\xi\varphi^3\chi^4 \\
& \times \sqrt{r^2\chi} - 432r^8s\zeta\xi\varphi^3\chi^4\sqrt{r^2\chi} - 80r^8\xi^3\varphi\chi^4\sqrt{r^2\chi} + 32r^8s\xi^3\varphi\chi^4\sqrt{r^2\chi} \\
& - 384r^8\zeta\xi^3\varphi\chi^4\sqrt{r^2\chi} + 192r^6\zeta\xi^3\varphi\chi^4\sqrt{r^2\chi} - 64r^6s\zeta\xi^3\varphi\chi^4\sqrt{r^2\chi} + 4r^8 \\
& \times \xi\varphi^3\chi^3\sqrt{r^2\chi} + 56r^8s\xi\varphi^3\chi^3\sqrt{r^2\chi} - 64r^8\zeta\xi\varphi^3\chi^3\sqrt{r^2\chi} - 208r^6\zeta\xi\varphi^3\chi^3 \\
& \times \sqrt{r^2\chi} - 208r^6s\zeta\xi\varphi^3\chi^3\sqrt{r^2\chi} + 384r^8\xi^3\varphi\chi^3\sqrt{r^2\chi} - 6r^6\xi^3\varphi\chi^3\sqrt{r^2\chi} \\
& + 60r^6s\xi^3\varphi\chi^3\sqrt{r^2\chi} - 128r^6\zeta\xi^3\varphi\chi^3\sqrt{r^2\chi} + 64r^4\xi\varphi^3\chi^3\sqrt{r^2\chi} - 1088 \\
& \times r^4s\xi\varphi^3\chi^3\sqrt{r^2\chi} + 32\xi^3\varphi\sqrt{r^2\chi} + 6r^{19}\varphi^4\chi^7 + 16r(3s-1)\xi^4\chi + r^{17} \\
& \times \chi^6(11 - 18\zeta\chi) - h\kappa r(\chi r^2 + 1)^4(8r^3\xi\varphi^3(r^2\chi)^{3/2} + r\xi^3\varphi\sqrt{r^2\chi} + \xi^4
\end{aligned}$$

$$\begin{aligned}
& + r^8 \varphi^4 \chi^2 + 24r^4 \xi^2 \varphi^2 \chi) - 4\mathcal{B}_g \kappa r s (\chi r^2 + 1)^4 (8r^3 \xi \varphi^3 (r^2 \chi)^{3/2} + 32r \xi^3 \\
& \times \sqrt{r^2 \chi} + 16 \xi^4 + r^8 \varphi^4 \chi^2 + 24r^4 \xi^2 \varphi^2 \chi) - 16r^3 \xi^2 \chi (\chi (-7s + 4(5s - 3) \\
& \times \zeta \chi + 4) \xi^2 + \varphi^2 (8\zeta \chi - 3)) + r^{15} \varphi^2 \chi^5 (\chi \xi^2 + \varphi^2 ((s - 4\zeta - 4) \chi + 30)) \\
& + r^9 \chi^3 (32\chi (3 - 2\zeta \chi) \xi^4 - \varphi^2 (2(7s - 18) \zeta \chi^2 + (6 - 5s + 16\zeta) 3\chi - 30) \\
& \times \xi^2 + \varphi^4 (3(s + 3) - 8(4s + 7) \zeta \chi)) + 8r^5 \xi^2 \chi^2 (2(\chi (\zeta \chi s + 5s - 5) + 2) \\
& \times \xi^2 + \varphi^2 (-56\zeta \chi s + 9s - 20\zeta \chi + 12)) + 4r^7 \chi^2 (4\chi ((s - 4\zeta - 2) \chi + 6) \\
& \times \xi^4 + 2\varphi^2 (\chi (21s - 8\zeta + (1 - 2s) \zeta \chi - 3) + 6) \xi^2 + \varphi^4 (1 - 8\zeta \chi)) + r^{13} \\
& \times \varphi^2 \chi^4 (16\chi (21 - 22\zeta \chi) \xi^2 + \varphi^2 (\chi (5s - 64\zeta - 6(s - 4) \zeta \chi - 7) + 18)) \\
& + r^{11} \chi^3 (32\chi^2 \xi^4 + 24\varphi^2 \chi ((s - 28\zeta - 3) \chi + 18) \xi^2 + \varphi^4 (\chi (-60\zeta \chi s + 7s \\
& - 16\zeta + 12\zeta \chi + 2) + 4))) \Big] \Big[ \kappa (3s - 1) (\chi r^2 + 1)^4 (r^2 \varphi^2 (r^2 \chi)^{3/2} + 4\xi^2 \\
& \times \sqrt{r^2 \chi} + 4r^3 \xi \varphi \chi)^2 \Big]^{-1}. \tag{B5}
\end{aligned}$$

## Appendix C: Boundary Condition at the Stellar Surface

To maintain physical continuity, the radial pressure must vanish at the boundary of the star, i.e.,  $p_r(R) = 0$ . By applying the linear equation of state  $p_r = s\rho - h$  and substituting the expressions for  $B_1$  and  $B_2$  into the resulting field equations, we derive the following explicit expression for the constant  $h$

$$\begin{aligned}
h = & - \Big[ s (64\xi^4 (16\mathcal{B}_g \kappa \xi^2 + \chi (16\zeta \chi - 5) \xi^2 + 3\varphi^2 (5 - 8\zeta \chi)) (r^2 \chi)^{3/2} - 32 \\
& \times r^2 \xi^4 (\chi (4(\chi (\zeta \chi - 5) + 3) \xi^2 + 3\varphi^2 (25 - 44\zeta \chi)) - (8\chi \xi^2 + 5\varphi^2) 6B\kappa) \\
& \times (r^2 \chi)^{3/2} + 16r^2 \xi^2 (4\chi (16\mathcal{B}_g \kappa + 12\zeta \chi + 5\chi - 18) \xi^4 + 3\varphi^2 (80\mathcal{B}_g \kappa + \chi \\
& \times (8\zeta (2 - 15\chi) - 5) - 20) \xi^2 + 6\varphi^4 (24\zeta \chi - 5)) (r^2 \chi)^{5/2} + 16r^4 \xi^2 (\mathcal{B}_g \kappa \\
& \times (16\chi^2 \xi^4 + 360\varphi^2 \chi \xi^2 + 15\varphi^4) + \chi (24\chi (2\zeta \chi - 3) \xi^4 - 6(\chi (53\chi \zeta - 64 \\
& \times \zeta - 30) + 55) \varphi^2 \xi^2 + \varphi^4 (316\zeta \chi - 75))) (r^2 \chi)^{5/2} - 4r^4 (96\chi^2 \xi^6 - 12 \\
& \times \varphi^2 \chi (80B\kappa + 268\zeta \chi + 35\chi - 210) \xi^4 + \varphi^4 (-240\mathcal{B}_g \kappa + \chi (32\zeta (5\chi - 9) \\
& + 105) + 120) \xi^2 + 3\varphi^6 (1 - 8\zeta \chi)) (r^2 \chi)^{7/2} - 18r^{22} \varphi^6 \chi^8 \sqrt{r^2 \chi} + 256\mathcal{B}_g \kappa
\end{aligned}$$

$$\begin{aligned}
& \times \xi^6 \sqrt{r^2 \chi} + 2r^{20} \varphi^6 \chi^7 (2\mathcal{B}_g \kappa + 54\zeta \chi - 33) \sqrt{r^2 \chi} + r^{18} \varphi^4 \chi^6 (\varphi^2 (16\mathcal{B}_g \kappa \\
& + 252\zeta \chi + 11\chi - 90) - 840\xi^2 \chi) \sqrt{r^2 \chi} + 2r^{16} \varphi^4 \chi^5 (12\chi (10\mathcal{B}_g \kappa + 158 \\
& \times \zeta \chi - 125) \xi^2 + \varphi^2 (12\mathcal{B}_g \kappa + \chi (-33\chi \zeta + 96\zeta + 8) - 27)) \sqrt{r^2 \chi} + r^{14} \\
& \times \varphi^2 \chi^4 (-2400\chi^2 \xi^4 + 12\varphi^2 \chi (80\mathcal{B}_g \kappa + 668\zeta \chi + 45\chi - 330) \xi^2 + \varphi^4 \\
& \times (16\mathcal{B}_g \kappa + \chi (24\zeta (\chi + 2) - 13) - 12)) \sqrt{r^2 \chi} + 2r^{12} \varphi^2 \chi^3 (2\mathcal{B}_g \kappa (24\chi^2 \\
& \times \xi^4 + 360\varphi^2 \chi \xi^2 + \varphi^4) + \chi (48\chi (78\zeta \chi - 85) \xi^4 + 4\varphi^2 (\chi (319\chi \zeta + \zeta \\
& \times 672 + 105) - 285) \xi^2 + 5\varphi^4 (20\zeta \chi - 3))) \sqrt{r^2 \chi} - 192r^{21} \xi \varphi^5 \chi^8 - 3 \\
& \times r \xi^5 \varphi \chi + 24r^{19} \xi \varphi^5 \chi^7 (2\mathcal{B}_g \kappa + 42\zeta \chi - 29) + 64r^3 \xi^5 \varphi \chi (12\mathcal{B}_g \kappa + \chi \\
& \times (8\zeta \chi - 15)) + 24r^{17} \xi \varphi^3 \chi^6 (\varphi^2 (8\mathcal{B}_g \kappa + 94\zeta \chi + 5\chi - 39) - 80\xi^2 \chi) \\
& + 64r^5 \xi^3 \varphi \chi^2 ((68\zeta \chi^2 + 6\chi + 48\mathcal{B}_g \kappa - 6) \xi^2 + 3\varphi^2 (16\zeta \chi - 5)) + 8r^9 \\
& \times \xi \varphi \chi^3 (48\chi (8\mathcal{B}_g \kappa + 14\zeta \chi + 3\chi - 15) \xi^4 + 8\varphi^2 (40\mathcal{B}_g \kappa - 2\chi (225\chi \zeta \\
& - 12\zeta + 5) - 15) \xi^2 + 3\varphi^4 (32\zeta \chi - 5)) + 4r^{15} \xi \varphi^3 \chi^5 (16\chi (10\mathcal{B}_g \kappa + \zeta \\
& \times 114\chi - 105) \xi^2 + 3\varphi^2 (24\mathcal{B}_g \kappa + \chi (-54\chi \zeta + 136\zeta + 15) - 46)) + 8 \\
& \times r^{13} \xi \varphi \chi^4 (-192\chi^2 \xi^4 + 8\varphi^2 \chi (40\mathcal{B}_g \kappa + 222\zeta \chi + 20\chi - 135) \xi^2 + 3 \\
& \times \varphi^4 (8\mathcal{B}_g \kappa + \chi (2\zeta (\chi + 8) - 5)) + 4r^{11} \xi \chi^3 (12\mathcal{B}_g \kappa \varphi (16\chi^2 \xi^4 + 8 \\
& \times \varphi^2 \chi \xi^2 + \varphi^4) + \chi (3(136\zeta \chi - 25) \varphi^5 - 8\xi^2 (\chi (158\chi \zeta - 264\zeta - 65) \\
& + 150) \varphi^3 + 96\xi^4 \chi (10\zeta \chi - 13) \varphi)) + 32r^7 \xi^3 \varphi \chi^2 (4\mathcal{B}_g \kappa (36\chi \xi^2 + 5\varphi^2) \\
& + \chi ((2\chi (34\chi \zeta + 24\zeta + 33) - 4) \xi^2 + \varphi^2 (24\zeta \chi - 75)))) \Big] \Big[ \kappa (\chi r^2 + 1)^4 \\
& \times (24r^2 \xi^4 \varphi^2 (r^2 \chi)^{3/2} + 60r^4 \xi^2 \varphi^4 (r^2 \chi)^{5/2} + 64\xi^6 \sqrt{r^2 \chi} + \chi^3 \sqrt{r^2 \chi} r^{12} \\
& \times \varphi^6 + 12r^{11} \xi \varphi^5 \chi^3 + 160r^7 \xi^3 \varphi^3 \chi^2 + 192r^3 \xi^5 \varphi \chi) \Big]^{-1}. \quad (C1)
\end{aligned}$$

## Appendix D: Calculation of the Bounds of the Coupling Parameters

We determine the following limit for  $\zeta$

$$\begin{aligned}
\zeta & > \Big[ (\chi r^2 + 1)^2 \Big( [18r^8 \varphi^2 \chi^3 (r^2 \chi)^{3/2} + r^2 (2(3\varphi^2 - 2(4\mathcal{B}_g \kappa + 3h\kappa - 6) \xi^2) \chi \\
& - (4\mathcal{B}_g + 3h) \kappa \varphi^2) (r^2 \chi)^{3/2} - 4(\xi^2 (8\mathcal{B}_g \kappa + 6h\kappa + 5\chi) - 3\varphi^2) (r^2 \chi)^{3/2} \\
& + r^2 (24\xi^2 \chi - \varphi^2 (8B\kappa + 6h\kappa + 11\chi - 12)) (r^2 \chi)^{5/2} + (-4\mathcal{B}_g \kappa - 3h\kappa + 30)
\end{aligned}$$

$$\begin{aligned}
& \times r^8 \varphi^2 \chi^3 \sqrt{r^2 \chi} - 4(4\mathcal{B} + 3h)\kappa \xi^2 \sqrt{r^2 \chi} + 48r^9 \xi \varphi \chi^4 - 4(4\mathcal{B}_g \kappa + 3h\kappa - 18) \\
& \times r^7 \xi \varphi \chi^3 + 24r \xi \varphi \chi - 4r^3 \xi \varphi (4\mathcal{B}_g \kappa + 3h\kappa - 3\chi) \chi - 8r^5 \xi \varphi \chi^2 (4\mathcal{B}_g \kappa + 3h\kappa \\
& + 4\chi - 3) \left[ 54r^8 \varphi^2 \chi^3 (r^2 \chi)^{3/2} - 4(\xi^2 \chi - 25\varphi^2) (r^2 \chi)^{3/2} + 12r^2 (2\chi \xi^2 + \varphi^2 \right. \\
& \times (\chi + 2)) (r^2 \chi)^{3/2} + 3r^2 (8\chi \xi^2 + \varphi^2 (32 - 11\chi)) (r^2 \chi)^{5/2} + r^8 \varphi^2 \chi^3 \sqrt{r^2 \chi} \\
& + 16(3\varphi^2 - 2\xi^2 \chi) \sqrt{r^2 \chi} + 72r^9 \xi \varphi \chi^4 + 120r^7 \xi \varphi \chi^3 - 72r^3 \xi \varphi \chi^2 + 16r \xi \varphi \chi \\
& + 12r^5 \xi \varphi \chi^2 (4 - 5\chi) \right]^{-1} - [s(192\xi^5 \varphi (r^2 \chi)^{3/2} - 192r^2 \xi^3 \varphi (\xi^2 (6\chi - 2) - 5 \\
& \times \varphi^2) (r^2 \chi)^{3/2} + 480r^2 \xi^3 \varphi (4\xi^2 + \varphi^2) (r^2 \chi)^{5/2} + 8r^4 \xi \varphi (192\chi \xi^4 + 40\varphi^2 (3 \\
& - 4\chi) \xi^2 + 15\varphi^4) (r^2 \chi)^{5/2} + 60r^4 \xi \varphi^3 (48\xi^2 + \varphi^2) (r^2 \chi)^{7/2} + 192r^{16} \xi \varphi^5 \chi^5 \\
& \times \sqrt{r^2 \chi} + 312r^{14} \xi \varphi^5 \chi^4 \sqrt{r^2 \chi} + 384\xi^5 \varphi \sqrt{r^2 \chi} + 120r^{12} \xi \varphi^3 \chi^3 (16\xi^2 \chi - \varphi^2 \\
& \times (\chi - 1)) \sqrt{r^2 \chi} + 18r^{19} \varphi^6 \chi^6 + 30r^{17} \varphi^6 \chi^5 + 6r^{13} \varphi^4 (220\xi^2 + \varphi^2) \chi^4 + 240 \\
& \times r^9 \xi^2 \varphi^2 (14\xi^2 + \varphi^2) \chi^3 + 96r^5 \xi^4 (4\xi^2 + 5\varphi^2) \chi^2 - 320r^3 \xi^4 \chi (\xi^2 \chi - 3\varphi^2) \\
& + r^{15} \varphi^4 \chi^4 (840\chi \xi^2 + \varphi^2) + 48r^7 \xi^2 \chi^2 (8\chi \xi^4 + 5\varphi^2 (4 - 7\chi) \xi^2 + 10\varphi^4) + 2 \\
& \times r^{11} \varphi^2 \chi^3 (200\chi \xi^4 + 5\varphi^2 (8 - 9\chi) \xi^2 + \varphi^4) - 4\mathcal{B}_g \kappa r (\chi r^2 + 1)^2 (160r^3 \xi^3 \varphi^3 \\
& \times (r^2 \chi)^{3/2} + 12r^5 \xi \varphi^5 (r^2 \chi)^{5/2} + 192r \xi^5 \varphi \sqrt{r^2 \chi} + 64\xi^6 + r^{12} \varphi^6 \chi^3 + 60r^8 \\
& \times \xi^2 \varphi^4 \chi^2 + 240r^4 \xi^4 \varphi^2 \chi)) - h\kappa r (\chi r^2 + 1)^2 (160r^3 \xi^3 \varphi^3 (r^2 \chi)^{3/2} + 12r^5 \\
& \times \xi \varphi^5 (r^2 \chi)^{5/2} + 192r \xi^5 \varphi \sqrt{r^2 \chi} + 60r^8 \xi^2 \varphi^4 \chi^2 + 240r^4 \xi^4 \varphi^2 \chi) ] = \Psi,
\end{aligned}$$

where  $\Psi$  represents the lower bound obtained from the trace energy condition. Additionally, since the transverse sound velocity inside the star gives us another limit for  $\zeta$

$$\begin{aligned}
\zeta & < 1 + \left[ r^2 (2(3\varphi^2 - 2(4\mathcal{B}_g \kappa + 18r^8 \varphi^2 \chi^3 (r^2 \chi)^{3/2} + 3h\kappa - 6) \xi^2) \chi + 30\mathcal{B}_g \kappa \right. \\
& - (4\mathcal{B}_g + 3h) \kappa \varphi^2) (r^2 \chi)^{3/2} - 4(\xi^2 (8\mathcal{B}_g \kappa + 6h\kappa + 5\chi) - 3\varphi^2) (r^2 \chi)^{3/2} \\
& + r^2 (24\xi^2 \chi - \varphi^2 (8\mathcal{B}_g \kappa + 6h\kappa + 11\chi - 12)) (r^2 \chi)^{5/2} + (-4\mathcal{B}_g \kappa - 3h\kappa) \\
& \times r^8 \varphi^2 \chi^3 \sqrt{r^2 \chi} - 4(4\mathcal{B} + 3h) \kappa \xi^2 \sqrt{r^2 \chi} + 48r^9 \xi \varphi \chi^4 - 4(4\mathcal{B}_g \kappa + 3h\kappa - 18) \\
& \times r^7 \xi \varphi \chi^3 + 24r \xi \varphi \chi - 4r^3 \xi \varphi (4\mathcal{B}_g \kappa + 3h\kappa - 3\chi) \chi - 8r^5 \xi \varphi \chi^2 (4\mathcal{B}_g \kappa + 3h\kappa \\
& \times r^{11} \varphi^2 \chi^3 (200\chi \xi^4 + 5\varphi^2 (8 - 9\chi) \xi^2 + \varphi^4) - 4\mathcal{B}_g \kappa r (\chi r^2 + 1)^2 (160r^3 \xi^3 \varphi^3 \\
& \times (r^2 \chi)^{3/2} + 12r^5 \xi \varphi^5 (r^2 \chi)^{5/2} + 192r \xi^5 \varphi \sqrt{r^2 \chi} + 64\xi^6 + r^{12} \varphi^6 \chi^3 + 60r^8 \\
& \times \xi^2 \varphi^4 \chi^2 + 240r^4 \xi^4 \varphi^2 \chi)) - h\kappa r (\chi r^2 + 1)^2 - 4\mathcal{B}_g \kappa r (\chi r^2 + 1)^2 24\xi^2
\end{aligned}$$

$$\begin{aligned}
& \times r^9 \xi^2 \varphi^2 (14 \xi^2 + \varphi^2) \chi^3 + 96 r^5 \xi^4 (4 \xi^2 + 5 \varphi^2) \chi^2 - 320 r^3 \xi^4 \chi (\xi^2 \chi - 3 \varphi^2) \\
& + r^{15} \varphi^4 \chi^4 (840 \chi \xi^2 + \varphi^2) + 48 r^7 \xi^2 \chi^2 (8 \chi \xi^4 + 5 \varphi^2 (4 - 7 \chi) \xi^2 + 10 \varphi^4) + 2 \\
& \times r^{11} \varphi^2 \chi^3 (200 \chi \xi^4 + 5 \varphi^2 (8 - 9 \chi) \xi^2 + \varphi^4) - 4 \mathcal{B}_g \kappa r (\chi r^2 + 1)^2 (160 r^3 \xi^3 \varphi^3 \\
& \times (r^2 \chi)^{3/2} + 12 r^5 \xi \varphi^5 (r^2 \chi)^{5/2} + 192 r \xi^5 \varphi \sqrt{r^2 \chi} + 64 \xi^6 + r^{12} \varphi^6 \chi^3 + 60 r^8 \\
& + 4 \chi - 3) \left[ 54 r^8 \varphi^2 \chi^3 (r^2 \chi)^{3/2} - 4 (\xi^2 \chi - 25 \varphi^2) (r^2 \chi)^{3/2} + 12 r^2 (2 \chi \xi^2 + \varphi^2 \right. \\
& \times (\chi + 2) (r^2 \chi)^{3/2} + 3 r^2 (8 \chi \xi^2 + \varphi^2 (32 - 11 \chi)) (r^2 \chi)^{5/2} + r^8 \varphi^2 \chi^3 \sqrt{r^2 \chi} \\
& + 16 (3 \varphi^2 - 2 \xi^2 \chi) \sqrt{r^2 \chi} + 72 r^9 \xi \varphi \chi^4 + 120 r^7 \xi \varphi \chi^3 - 72 r^3 \xi \varphi \chi^2 + 16 r \xi \varphi \chi \\
& \left. + 12 r^5 \xi \varphi \chi^2 (4 - 5 \chi) \right]^{-1} = 1 + \Phi.
\end{aligned}$$

Here,  $1 + \Phi$  represents the upper bound derived from the sound velocity constraint.

**Data Availability Statement:** No data was used for the research described in this paper.

## References

- [1] Riess, A.G. et al.: *Astron. J.* **116**(1998)1009; Eisenstein, D.J. et al.: *Astrophys. J.* **633**(2005)560; Komatsu, E. et al.: *Astrophys. J. Suppl.* **180**(2009)330.
- [2] Beutler, F. et al.: *Mon. Not. Roy. Astron. Soc.* **416**(2011)3017; Betoule, M. et al.: *Astron. Astrophys.* **568**(2014)32; Ade, P. et al.: *Astron. Astrophys.* **594**(2016)28; Aghanim, N. et al.: *Astron. Astrophys.* **594**(2016)99.
- [3] Cartan, É.: *C.R. and Acad. Sci. Paris* **174**(1922)593.
- [4] Weitzenböck, R.: *Invariантentheorie* (Noordhoff, Groningen, 1923); Möller, C. and Dan, K.: *Mat. Fys. Skr.* **1**(1961)10; Pellegrini, C. and Plebanski, J.: *K. Dan. Vidensk. Selsk., Mat. Fys. Skr.* **2**(1963)4; Hayashi, K. and Shirafuji, T.: *Phys. Rev. D* **19**(1979)3524.
- [5] Nester, J.M. and Yo, H.-J.: *Chin. J. Phys.* **37**(1999)113; Adak, M., Kalay, M. and Sert, O.: *Int. J. Mod. Phys. D* **15**(2006)619.

- [6] Jiménez, J.B., Heisenberg, L. and Koivisto, T.: Phys. Rev. D **98**(2018)044048; Delhom-Latorre, A., Olmo, G.J. and Ronco, M.: Phys. Lett. B **780**(2018)294; Harko, T. et al.: Phys. Rev. D **98**(2018)084043.
- [7] Jiménez, J.B., Heisenberg, L. and Koivisto, T.: Universe **5**(2019)173; Jiménez, J.B. et al.: Phys. Rev. D **101**(2020)103507.
- [8] Abbas, G. and Nazar, H.: Ann. Phys. **424**(2021)168336.
- [9] Frolov, A.V.: Phys. Rev. Lett. **101**(2008)061103; Reverberi, L.: Phys. Rev. D **87**(2013)084005.
- [10] Saha, P. and Debnath, U.: Adv. High Energy Phys. **2018**(2018)3901790.
- [11] Camera, S., Cardone, V.F. and Radicella, N.: Phys. Rev. D **89**(2014)083520.
- [12] Anagnostopoulos, F.K. et al.: Phys. Lett. B **822**(2021)136634.
- [13] Frusciante, N.: Phys. Rev. D **103**(2021)044021.
- [14] Mandal, S., Parida, A. and Sahoo, P.K.: Universe **8**(2022)240.
- [15] Wang, W., Chen, H. and Katsuragawa, T.: Phys. Rev. D **105**(2022)024060.
- [16] D'Ambrosio, F. et al.: Phys. Rev. D **105**(2022)024042.
- [17] Gadbail, G.N., Mandal, S. and Sahoo, P.K.: Phys. Lett. B **835**(2022)137509.
- [18] De, A. and Loo, T.H.: Class. Quantum Grav. **40**(2023)115007; Khyllep, W. et al.: Phys. Rev. D **107**(2023)044022; Koussour, M. et al.: Prog. Theor. Exp. Phys. **2023** (2023)113E01; Sharif, M. and Ajmal, M.: Chin. J. Phys. **88**(2024)706; Phys. Scr. **99**(2024)085039; Phys. Dark Universe **46**(2024)101572; Astropart. Phys. **165**(2025)103054 Sharif, M., Gul, M.Z. and Fatima, N.: New Astron. **109**(2024)102211; Gadbail, G.N., Mandal, S. and Sahoo, P. K.: Astrophys. J. **972**(2024)174.
- [19] Zhang, C. and Ren, J.: Phys. Rev. D **108**(2023)063012.
- [20] Mishra, H. et al.: Int. J. Mod. Phys. E **2**(1993)547.

- [21] Khadkikar, S.B., Mishra, A. and Mishra, H.: *Mod. Phys. Lett. A* **10**(1995)2651.
- [22] Maheswari, V.U. et al.: *Nucl. Phys. A* **615**(1997)516.
- [23] Schertler, K. et al.: *Nucl. Phys. A* **637**(1998)451.
- [24] Blackman, E.G., Frank, A. and Welch, C.: *Astrophys. J.* **546**(2001)288.
- [25] Gupta, V. K., Tuli, V. and Goyal, A.: *Astrophys. J.* **579**(2002)374.
- [26] Grigorian, H., Blaschke, D. and Aguilera, D.N.: *Phys. Rev. C-Nucl. Phys.* **69**(2004)065802.
- [27] Alford, M. et al.: *Astrophys. J.* **629**(2005)969.
- [28] Nicotra, O.E. et al.: *Phys. Rev. D* **74**(2006)123001.
- [29] Hussain, H. et al.: *J. Polym. Sci. Polym. Chem.* **46**(2008)7287.
- [30] Dexheimer, V., Negreiros, R. and Schramm, S.: *Eur. Phys. J. A* **48**(2012)1.
- [31] Alford, M.G., Han, S. and Prakash, M.: *Phys. Rev. D* **88**(2013)083013.
- [32] Bhar, P.: *Astrophys. Space Sci.* **357**(2015)1.
- [33] Burgio, G.F. and Zappala, D.: *Eur. Phys. J. A* **52**(2016)60.
- [34] Kaltenborn, M.A.R., Bastian, N.U.F. and Blaschke, D.B.: *Phys. Rev. D* **96**(2017)056024.
- [35] Nandi, R. and Char, P.: *Astrophys. J.* **857**(2018)12.
- [36] Khanmohamadi, S., Moshfegh, H.R. and Tehrani, S.A.: *Phys. Rev. D* **101**(2020)023004.
- [37] Laskos-Patkos, P., Koliogiannis, P.S. and Moustakidis, C.C.: *Phys. Rev. C* **109**(2024)063017; Mariani, M. et al.: *Phys. Rev. C* **110**(2024)043026; Rigtering, C. et al.: *J. Bus. Res.* **176**(2024)114596; Li, J.J., Sedrakian, A. and Alford, M.: *Astrophys. J.* **967**(2024)116.
- [38] Bhar, P. et al.: *Eur. Phys. J. C* **83**(2023)737.

- [39] Rej, P.: Chin. J. Phys. **89**(2024)174.
- [40] Finch, M.R. and Skea, J.E.F.: Class. Quantum Grav. **6**(1989)467.
- [41] Hansraj, S. et al.: Int. J. Mod. Phys. D **15**(2006)1311; Banerjee, A. et al.: Gen. Relativ. Gravit. **45**(2013)717.
- [42] Sharma, R. and Ratanpal, B.S.: Int. J. Mod. Phys. D **22**(2013)1350074.
- [43] Sharma R. and Das S.: J. Gravit. **2013**(2013)659605.
- [44] Pandya D.M., Thomas V.O. and Sharma R.: Astrophys. Space Sci. **356**(2015)285.
- [45] Molina, A., Dadhich, N. and Khugaev, A.: Gen. Relativ. Gravit. **49**(2017)1.
- [46] Banerjee, A., Jasim, M.K. and Pradhan, A.: Mod. Phys. Lett. A **35**(2020)2050071.
- [47] Dayanandan, B. et al.: Chin. J. Phys. **82**(2023)155.
- [48] Gul, M.Z. et al.: Eur. Phys. J. C **84**(2024)8.
- [49] Mustafa, G. et al.: Chin. J. Phys. **88**(2024)954.
- [50] Rej, P., Bogadi, R.S. and Govender, M.: Chin. J. Phys. **87**(2024)608.
- [51] Shahzad, M.R. et al.: Phys. Dark Universe **46**(2024)101646.
- [52] Das, B. et al.: Astrophys. Space Sci. **369**(2024)76.
- [53] Weyl, H.: Sitzungsber. Preuss. Akad. Wiss. **465**(1918)01; Dirac, P.A.M.: Proc. R. Soc. London A **333**(1973)403.
- [54] Schertler, K. et al.: Nucl. Phys. A **677**(2000)463; Yan, Y. et al.: Phys. Rev. D **86**(2012)114028.
- [55] Mandal, S., Sahoo, P.K. and Santos, J.R.: Phys. Rev. D **102**(2020)024057.
- [56] Khyllep, W., Paliathanasis, A. and Dutta, J.: Phys. Rev. D **103**(2021)103521.

- [57] Lin, R.H. and Zhai, X.H.: Phys. Rev. D **103**(2021)124001.
- [58] Zhao, D.: Eur. Phys. J. C. **82**(2022)303.
- [59] Sharma, R. and Maharaj, S.D.: Mon. Not. R. Astron. Soc. **375**(2007)1265; Ngubelanga, S.A., Maharaj, S.D. and Ray, S.: Astrophys. Space Sci. **357**(2015)1; Abbas, G. and Nazar, H.: Ann. Phys. **424**(2021)168336.
- [60] Cheng, K.S., Dai, Z.G. and Lu, T.: Int. J. Mod. Phys. D **7**(1998)139.
- [61] Chodos, A.: Phys. Rev. D **9**(1974)3471.
- [62] Witten, E.: Phys. Rev. D **30**(1984)272.
- [63] Farhi, E. and Jaffe, R.L.: Phys. Rev. D **30**(1984)2379.
- [64] Peshier, A., Kampfer, B. and Soff, B.: Phys. Rev. C **61**(2000)045203.
- [65] Rehberg, P., Klevansky, S.P. and Hüfner, J.: Phys. Rev. C **53**(1996)410. Hanauske, M. et al.: Phys. Rev. D **64**(2001)043005; Rüster, S.B. and Rischke, D.H.: Phys. Rev. D **69**(2004)045011; Menezes, D.P., Providência, C. and Melrose, D.B.: J. Phys. G: Nucl. Part. Phys. **32**(2006)1081; Jiang, Y. et al.: Phys. Rev. D **85**(2012)034031.
- [66] Baluni, V.: Phys. Rev. D **17**(1978)2092; Fraga, E.S., Pisarski, R.D. and Schaffner-Bielich, J.: Phys. Rev. D **63**(2001)121702.
- [67] Aghanim, N. et al.: Astron. Astrophys. **652**(2021)C4.
- [68] Deb, D. et al.: Mon. Not. R. Astron. Soc. **485**(2019)5652; Rahaman, F. et al.: Phys. Rev. D **82**(2010)104055; Kalam, M. et al. : Eur. Phys. J. C **72**(2012)2248; Rahaman, F. et al.: Gen. Relativ. Gravit. **44**(2012)107.
- [69] O'Brien, S. and Synge, J.L.: Commun. Dublin Inst. Adv. Stud. **9**(1952)1.
- [70] Özel, F., Güver, T. and Psaltis, D.: Astrophys. J. **693**(2009)1775.
- [71] Rawls, M.L. et al.: Astrophys. J. **730**(2011)25.
- [72] Hell, T. and Weise, W.: Phys. Rev. C **90**(2014)045801.
- [73] Buchdahl, A.H.: Phys. Rev. D **116**(1959)1027.

- [74] Barraco, D.E. and Hamity, V.H.: Phys. Rev. D **65**(2002)124028.
- [75] Gadbail, G.N., Mandal, S. and Sahoo, P.K.: Physics **4**(2022)1403.
- [76] Abreu, H., Hernández, H. and Námez, L.A.: Class. Quantum Grav. **24**(2007)4631.
- [77] Chandrasekhar, S.: Astrophys. J. **140**(1964)417; Chan, R., Herrera, L. and Santos, N.: Mon. Not. R. Astron. Soc. **265**(1993)533.
- [78] Tolman, R.C.: Phys. Rev. **35**(1930)896; Tolman, R.C.: Phys. Rev. **55**(1939)364; Oppenheimer, J.R. and Volkoff, G.M.: Phys. Rev. **55**(1939)374.
- [79] Bhar, P., Malik, A. and Almas, A.: Chin. J. Phys. **88**(2024)839; Bhar, P. and Pretel, J.M.: Phys. Dark Universe **42**(2023)101322; Kaur, S. et al.: New Astron. **110**(2024)102230.
- [80] Bhar, P. et al.: Phys. Dark Universe **46**(2024)101686.
- [81] Nazar, H. and Abbas, G.: Adv. Astron. **2021**(2021)6698208.
- [82] Sharif, M. and Ibrar, I.: Chin. J. Phys. **89**(2024)1578; Eur. Phys. J. Plus **139**(2024)1; Phys. Scr. **99**(2024)105034.